Evolution of collective and noncollective structures in ^{123}Xe

Anwesha Basu and A. K. Singh
Department of Physics, Indian Institute of Technology Kharagpur, Kharagpur 721302, India

S. Nag
Department of Physics, Indian Institute of Technology (BHU), Varanasi 221005, India

G. B. Hagemann, G. Sletten, and B. Herskind
Niels Bohr Institute, Blegdamsvej 17, DK-2100 Copenhagen Ø, Denmark

A. N. Wilson* and J. Rogers
R. S. P. E., ANU, Canberra, ACT 0200, Australia

I. Ragnarsson
Division of Mathematical Physics, LTH, Lund University, Box 118, SE-221 00 Lund, Sweden

H. Hübel and S. Chmel†
Helmholtz-Institut für Strahlen- und Kernphysik, Universität Bonn, Nussallee 14-16, D-53115 Bonn, Germany

R. V. F. Janssens
Department of Physics and Astronomy, University of North Carolina at Chapel Hill, Chapel Hill, North Carolina 27599, USA
and Triangle Universities Nuclear Laboratory, Duke University, Durham, North Carolina 27708, USA

M. P. Carpenter, T. L. Khoo, F. G. Kondev, T. Lauritsen, and S. Zhu
Physics Division, Argonne National Laboratory, Argonne, Illinois 60439, USA

A. Korichi
CSNSM-IN2P3, F-91405 Orsay Campus, France

P. Fallon
Nuclear Science Division, Lawrence Berkeley National Laboratory, Berkeley, California 94720, USA

B. M. Nyakó and J. Timár
Institute for Nuclear Research, Hungarian Academy of Sciences, H-4001 Debrecen, Hungary

An experiment involving a heavy-ion-induced fusion-evaporation reaction was carried out where high-spin states of ^{123}Xe were populated in the ^{80}Se(^{48}Ca, $5n$)^{123}Xe reaction at 207 MeV beam energy. Gamma-ray coincidence events were recorded with the Gammasphere Ge detector array. The previously known level scheme was confirmed and enhanced with the addition of five new band structures and several interband transitions. Cranked Nilsson-Strutinsky (CNS) calculations were performed and compared with the experimental results in order to assign configurations to the bands.

I. INTRODUCTION

The transitional nuclei lying between the spherical Sn ($Z = 50$) and the deformed Ce ($Z = 58$) isotopes in the nuclear chart are susceptible to deformation changes and, therefore, exhibit a rich variety of structures and deformation effects. Shape changes, from prolate to oblate via triaxial, are observed in these nuclei by excitation of nucleons to various

---

*Present address: Faculty of Social Sciences, University of Stirling, Stirling FK9 4LA, United Kingdom.

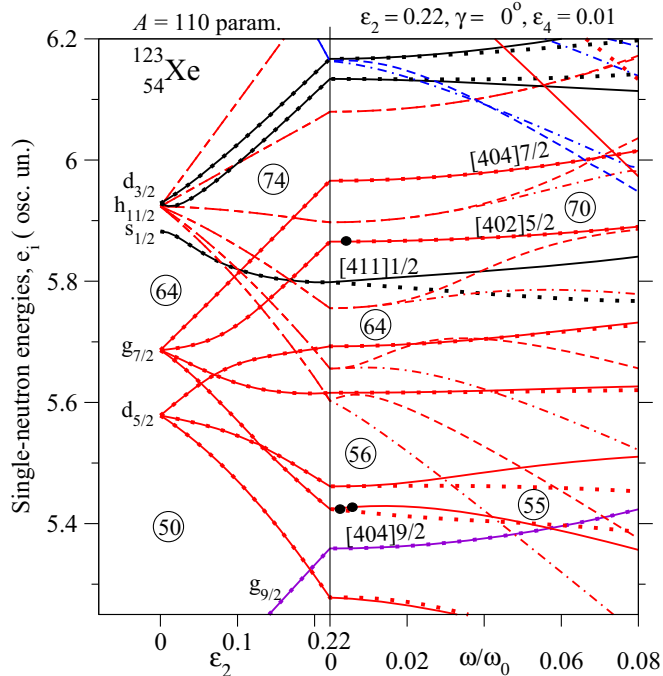†Present address: Fraunhofer INT, Appelsgarten 2, D-53879 Euskirchen, Germany.

FIG. 1. Single-particle neutron energies at a prolate shape as a function of the deformation parameter ε_2 (left part) and as a function of the rotational frequency at $\varepsilon_2 = 0.22$ (right part). Note that, for a larger quadrupole deformation and/or rotational frequency, it will be advantageous to create proton holes in the $g_{9/2}$ shell of the $Z = 50$ core, leading to configurations of larger collectivity [17,22–24]. Negative-parity orbitals are drawn by dashed lines while dots are used for signature $\alpha = -1/2$ orbitals, i.e., full lines are used for $(\pi, \alpha) = (+, +1/2)$, dots for $(+, -1/2)$, dashed lines for $(-, +1/2)$, and dashed-dotted lines for $(-, -1/2)$.

deformation-driving orbitals [1,2]. In the $A = 125$ mass region, the unique-parity intruder orbital $h_{11/2}$ is accessible to both protons and neutrons. Figure 1 displays the energy levels calculated by using the modified oscillator potential [3], where $A = 110$ parameters have been used [4]. For a general understanding of the valence space orbitals, this diagram can be used also for protons. Thus, in addition to the orbital of the odd neutron in the ground state for $N = 69$, the orbital occupied by the last proton pair for $Z = 54$ is indicated. The neutron Fermi surface, which controls the extent of triaxiality, lies in the middle to upper part of the shell, whereas the proton Fermi surface lies in the lower part. In the low- and medium-spin region, the protons and neutrons in $h_{11/2}$ orbitals have opposite deformation-driving effects. Nuclei are driven towards a prolate shape when the $h_{11/2}$ protons get aligned due to rotation-induced Coriolis effects, whereas an oblate shape is favored after the alignment of $h_{11/2}$ neutrons [1]. This interplay produces quite interesting shape coexistence effects [1,2,5–12].

In this mass region, it is favorable to consider ^{114}Sn as the closed core so that low-lying, oblate, fully aligned states are formed at the $I_{\max}$ values of the respective configurations formed from the valence nucleons. As seen in Fig. 1, for ^{123}Xe, this corresponds to four valence protons and five

valence neutrons above the $Z = 50$ and $N = 64$ shell gaps. Using the available j shells, a maximum spin around or just above $I = 30$ is easily achievable with the possible configurations. The evolution with spin makes it possible to investigate the interaction between configurations with low or no collectivity. Another interesting aspect is the similarity between the availability of the neutron orbitals for nuclei above a ^{114}Sn core ($Z = 50$, $N = 64$) with that of the proton orbitals above a ^{146}Gd core ($Z = 64$, $N = 82$) along with their distribution in these two mass regions [7,13]. In the $A = 150$–160 mass region, band termination has been observed [13,14]. The interplay between single-particle and collective excitations has been studied in detail in Refs. [10,14,15]. Maximally aligned states, with 8 to 11 particles, have been reported recently in Te and I isotopes as well [16–21]. In addition, noncollective states where the angular momentum of one or two particles are anti-aligned with respect to the rotation axis formed by the valence particles have been observed in ^{120}Te [16], and ^{123,125}I [18,19]. Several low-intensity, high-energy γ rays have been observed to feed maximally aligned states in ^{121}I [21], ^{123}I [18], ^{123}Cs [7], and ^{124}Ba [9]. Theoretical calculations suggest that these transitions originate from configurations involving excitations across the $N = 64$ core [7,9,18,19].

The structure of the Xe isotopes, other than that of ^{123}Xe, has been studied in great detail [10,12,22,25–27] and shape evolution with increasing rotational frequency has been reported. In addition, highly deformed rotational bands, extending up to spins around $I \sim 60$, have been observed to coexist along with "normally" deformed bands in the spin range $I = 20$–30 in ^{124,125,126}Xe [12,22,27]. Similar bands have been observed in other neighboring nuclei such as ^{120,122}Te [16,17] and ^{123,125}I [18,19].

In this article, the results obtained from high-spin γ-ray spectroscopy of the ^{123}Xe isotope are discussed. The previously known level scheme of this nucleus [28–30] has been considerably extended. Cranked Nilsson-Strutinsky (CNS) model calculations were performed to assign configurations to the observed structures.

The experimental details and the data analysis methods are presented in Sec. II. Section III deals with the experimental results and the partial level scheme that has been established in the present work. In Sec. IV, probable configurations assigned to the new band structures are discussed. This is followed by a brief summary of the current work in Sec. V.

II. EXPERIMENTAL DETAILS AND ANALYSIS

To study the high-spin states of ^{123}Xe, a heavy-ion induced fusion-evaporation reaction, ^{80}Se(^{48}Ca, 5n)^{123}Xe, was carried out at the Argonne National Laboratory. The ATLAS accelerator provided the ^{48}Ca beam of 207 MeV energy with an intensity of 4 pnA. The target consisted of ^{80}Se at 0.6 mg/cm^2 thickness evaporated on to a 0.3 mg/cm^2 Au backing. In addition, a 0.04 mg/cm^2 layer of Au was deposited on the Se foil for protection against sputtering. For heat dissipation, the target was mounted on a rotating wheel and the beam was wobbled horizontally and was slightly defocused. With these precautions, the target could withstand a maximum beam

intensity of 4 pnA over the period of the experiment. The Gammasphere spectrometer [31], consisting of 101 Compton-suppressed Ge detectors at the time of the experiment, was used to measure γ-ray coincidence relationships. A total of 2.7×10^9 events, with a Ge-detector coincidence fold $\geqslant 4$, were recorded over a beam time of 10 days. In this experiment, the high-spin levels of ^{123}Xe were populated with an intensity sufficient to carry out this study, even though the main motivation was to search for hyperdeformed structures in ^{124}Xe. The other strongly populated nuclei in the experiment were ^{124}Xe, ^{123}I, and ^{120}Te via the $4n$, $p4n$, and $\alpha4n$ channels, respectively. The results for ^{124}Xe [22], ^{123}I [18,24], and ^{120}Te [16] have already been published.

In the offline analysis, the raw data were presorted. The process includes Compton suppression, pile-up rejection, gain matching, and the calibration of the detectors. The RADWARE software package [32] was used to sort the γ-ray coincidence data into two-, three-, and four-dimensional arrays called matrices, cubes, and hypercubes, respectively.

To determine angular distribution ratios, the data were sorted into two matrices. In the first one, the events detected in the detectors mounted around forward (35°) and backward (145°) angles were placed on one axis (fb), whereas the other (all) contained events detected in all the detectors. Similarly, the second matrix had events detected in the detectors around 90° on one axis (90), and the events detected in all other detectors on the other axis (all). To determine the angular distribution ratios R_θ, gates were set on the (all) axes of the matrices. The intensity ratio is given by

$$R_\theta = \frac{I\left(\gamma_1^{fb}, \gamma_2^{\text{all}}\right)}{I\left(\gamma_1^{90}, \gamma_2^{\text{all}}\right)}, \tag{1}$$

and is used to distinguish between stretched dipole and stretched quadrupole transitions which have ≈ 0.6 and 1.4 respective values. The stretched quadrupole transitions were assumed to be of $E2$ multipolarity. The angular distribution ratio R_θ was determined from spectra gated on dipole as well as on quadrupole transitions. The difference in R_θ values with gates on dipole and quadrupole transitions were within 10% limits. This is expected for a symmetric array such as Gammasphere, where angular distribution effects are averaged out for gating transitions.

The relative intensities of γ rays have been determined from spectra produced with double or triple gates on transitions below the γ ray of interest. The relative intensities of γ rays listed in Table I have been normalized to that of the 616.6 keV γ ray of band 9 with $I_\gamma = 1000$. For some of the transitions of low-energy bands, e.g., 4, 5, 10, 11, 14, and 15, intensities could not be determined accurately due to unavailability of a reference γ ray for normalization.

III. RESULTS AND LEVEL SCHEME

Low- and high-spin states of ^{123}Xe were known from previous work [28,29]. Here, several new bands have been identified in the high-spin region, and the existing sequences have been extended. The γ-ray transitions with energies less than 100 keV were not observed in this experiment and

have been adopted from Ref. [33]. The updated ^{123}Xe level scheme is displayed in Fig. 2. The low-energy levels of Fig. 2 have been shown separately with an expanded energy scale in Fig. 3. The dipole band reported by Rainovski *et al.* [34] could not be confirmed in this experiment. Most of the transitions in this band are also present in one of the bands assigned to ^{124}I and intense transitions from this channel were observed in gated spectra. In the following sections, the results are summarized and the assignments of spin-parity quantum numbers to the levels are discussed.

A. Bands 1, 2, and 3

Band 1 was observed in the previous work by Schmidt *et al.* [29], although the spins and parity were tentatively assigned. In the present work, the in-band transitions are confirmed and the band is extended to spin 55/2. Two new bands, bands 2 and 3, have been observed. They are connected with band 1 and several decay-out transitions have been observed from these sequences to lower-energy levels. The lowest-energy level of band 1 at 3908 keV was tentatively assigned spin 27/2 in previous work [29]. Here, the angular distribution ratios R_θ measured for the 1138 and 739 keV decay-out transitions indicate their respective quadrupole and dipole nature (see Table I). Thus, a spin of 27/2 and negative parity have been assigned to the level. The assignment is also consistent with other decay-out transitions from this level. The R_θ values measured for some of the transitions of band 1 confirm their stretched quadrupole character. For these and the other in-band transitions, $E2$ multipolarity was assumed. Several interband transitions have been observed between bands 1 and 2, confirming the placements of Fig. 2. The dipole nature of some of these could be confirmed through the angular distribution ratio R_θ (see Table I).

Band 2 is newly observed and is most likely the signature partner of band 1. The R_θ ratio measured for the 376 keV γ ray connecting to band 1 shows its dipole nature. Therefore, spin 29/2 has been assigned to the lowest level of band 2. This state also decays by a transition at 934 keV to a level with known spin and parity of $27/2^+$ of band 13. The value $R_\theta = 0.74(9)$ is consistent with an $E1$ character for the transition. In addition, several $E1$ transitions, notably those of 757, 711, 871, 739, and 789 keV, decaying alternatively from bands 1 and 2 to the positive-parity bands 12 and 13, have been observed in the coincidence spectra.

Another cascade of transitions, marked as band 3, has been observed in coincidence with transitions of band 2. Altogether, bands 1–3 form a cluster of bands connected by dipole transitions. The parity for each of the bands has been tentatively assigned to be negative assuming that interband transitions are of $M1$ or $E2$ character. The gated spectra with γ rays of bands 1–3 are displayed in Fig. 4.

B. Bands 4 to 10

The levels of bands 4 and 5 were known from earlier work [29,30]. However, the spins and parity of some of the levels were not assigned. In the present work, several new γ rays, connecting bands 1, 2, and 9 to bands 4 and 5, have

TABLE I. Gamma-ray energies, level energies, intensities, spin assignments, angular distribution ratios, and multipolarities of γ-ray transitions of ^{123}Xe. The γ rays with energies less than 100 keV have been adopted from Ref. [28].

Energy E_γ (keV)[a]	Initial level energy E_i (keV)[b]	Intensity I_γ [c]	Spin assignment $I_i^\pi \to I_f^\pi$	Intensity ratio R_θ	Multipolarity assignment
21.1	206.2		$9/2^- \to 7/2^-$		
57.0	263.1		$11/2^- \to 9/2^-$		
66.8	251.9		$7/2^+ \to 7/2^-$		
71.4	251.9		$7/2^+ \to 5/2^+$		
77.9	263.1		$11/2^- \to 7/2^-$		
83.3	180.6		$5/2^+ \to 3/2^+$		
97.3	97.3		$3/2^+ \to 1/2^+$		
131.2	437.5		$7/2^+ \to 5/2^+$		
136.5	4155.4	19(3)	$31/2^+ \to 29/2^+$	0.52(5)	$M1 + E2$
139.4	3349.1	76(10)	$27/2^+ \to 25/2^+$	0.67(7)	$M1 + E2$
156.6	5036.2	20(3)	$35/2^+ \to 33/2^+$	0.56(6)	$M1 + E2$
180.4	3349.1	384(43)	$27/2^+ \to 25/2^+$	0.65(6)	$M1 + E2$
180.5	180.6		$5/2^+ \to 1/2^+$		
199.4	11089.3	17(2)	$59/2^- \to 57/2^-$	0.78(7)	$M1 + E2$
205.1	3168.7	167(24)	$25/2^+ \to 23/2^+$		
209.5	306.9		$5/2^+ \to 3/2^+$		
240.2	8693.5	7(1)	$49/2^+ \to 49/2^+$	1.07(12)	$M1 + E2$
249.0	767.5		$11/2^+ \to 9/2^+$		
255.1	518.1		$9/2^+ \to 11/2^-$	0.93(11)	$E1$
266.2	518.1		$9/2^+ \to 7/2^+$	0.63(6)	$M1 + E2$
266.3	2688.4		$21/2^+ \to 19/2^+$	0.49(6)	$M1 + E2$
275.3	2963.6		$23/2^+ \to 21/2^+$	0.63(7)	$M1 + E2$
287.0	3168.7	113(16)	$25/2^+ \to 23/2^+$	0.60(5)	$M1 + E2$
294.6	9418.7	10(2)	$53/2^+ \to 51/2^+$	0.48(4)	$M1 + E2$
306.9	306.9		$5/2^+ \to 1/2^+$		
312.2	518.1		$9/2^+ \to 9/2^-$		
314.2	1081.6		$13/2^+ \to 11/2^+$		
315.3	1397.4		$15/2^+ \to 13/2^+$		
324.6	6789.2	43(5)	$41/2^- \to 39/2^-$	0.68(5)	$M1 + E2$
325.4	4608.5		$31/2^- \to 29/2^-$		
333.3	518.1		$9/2^+ \to 7/2^-$		
335.2	4155.4	30(4)	$31/2^+ \to 29/2^+$	0.72(7)	$M1 + E2$
337.8	518.1		$9/2^+ \to 5/2^+$		
340.2	437.5		$7/2^+ \to 3/2^+$	1.23(13)	$E2$
347.0	3168.7	30(5)	$25/2^+ \to 23/2^+$		
363.1	1081.6		$13/2^+ \to 15/2^-$		
366.8	7481.4		$45/2^+ \to 43/2^+$	0.71(6)	$M1 + E2$
371.1	6789.2	19(2)	$41/2^- \to 39/2^-$	0.38(5)	$M1 + E2$
375.6	4283.3		$29/2^- \to 27/2^-$	0.64(6)	$M1 + E2$
382.9	6070.0	6(1)	$37/2^- \to 35/2^-$	0.67(13)	$M1 + E2$
385.1	3349.1	64(8)	$27/2^+ \to 23/2^+$		
392.6	1269.6		$15/2^- \to 13/2^-$		
394.8	6464.6	11(2)	$39/2^- \to 37/2^-$	0.68(5)	$M1 + E2$
396.3[d,e]	5915.4	196(24)	$39/2^+ \to 37/2^+$		
396.9[d,e]	7481.4		$45/2^+ \to 43/2^+$		
399.0	661.9		$13/2^- \to 11/2^-$		
401.3	5687.1		$35/2^- \to (33/2^-)$		
401.6	9356.4	169(20)	$53/2^- \to 49/2^-$	1.38(12)	$E2$
403.7	4354.9		$(31/2^-) \to 31/2^-$		
408.6	5036.2	17(2)	$35/2^+ \to 33/2^+$	0.72(8)	$M1 + E2$
417.8	5026.3	35(4)	$33/2^- \to 31/2^-$	0.67(7)	$M1 + E2$
430.1	9124.1	16(2)	$51/2^+ \to 49/2^+$	0.92(10)	$M1 + E2$
430.9	1953.1		$19/2^- \to 17/2^-$		
455.6	718.7		$15/2^- \to 11/2^-$		
455.7	661.9		$13/2^- \to 9/2^-$		
455.9	5793.4		$37/2^- \to 35/2^-$	0.68(7)	$M1 + E2$

TABLE I. (*Continued.*)

Energy E_γ (keV)[a]	Initial level energy E_i (keV)[b]	Intensity I_γ [c]	Spin assignment $I_i^\pi \to I_f^\pi$	Intensity ratio R_θ	Multipolarity assignment
457.6	8074.7		$47/2^- \to 45/2^-$		
462.7	8453.3	111(12)	$49/2^+ \to 47/2^+$	0.71(7)	$M1 + E2$
466.8	3349.1	28(4)	$27/2^+ \to 23/2^+$		
470.9[d,e]	3820.2	190(23)	$29/2^+ \to 27/2^+$		
471.4[d,e]	4627.6		$33/2^+ \to 31/2^+$		
480.3	3168.7	107(15)	$25/2^+ \to 21/2^+$	1.39(16)	$E2$
483.2	5519.1	109(13)	$37/2^+ \to 35/2^+$	0.88(10)	$M1 + E2$
484.3	2769.2		$23/2^- \to 21/2^-$		
497.0	934.5		$11/2^+ \to 7/2^+$		
504.1	8693.5	8(1)	$49/2^+ \to 47/2^+$	0.66(7)	$M1 + E2$
515.1	12235.8	15(3)	$63/2^- \to 61/2^-$	0.76(6)	$M1 + E2$
515.6	767.5		$11/2^+ \to 7/2^+$		
521.7	6654.9	43(6)	$41/2^- \to 39/2^-$	0.71(6)	$M1 + E2$
523.1	7780.3		$45/2^- \to 43/2^-$	0.84(8)	$M1 + E2$
534.8	12857.6		$\to$		
541.8	2963.6		$23/2^+ \to 19/2^+$	1.29(10)	$E2$
550.5	7616.8	22(3)	$45/2^- \to 43/2^-$	0.59(6)	$M1 + E2$
550.8	1269.6		$15/2^- \to 15/2^-$	0.71(7)	$M1 + E2$
555.7	3905.0	2.0(5)	$29/2^+ \to 27/2^+$		
558.4	5584.7		$35/2^- \to 33/2^-$	0.62(7)	$M1 + E2$
561.5	6476.8	308(36)	$41/2^+ \to 39/2^+$	0.59(6)	$M1 + E2$
563.5	1081.6		$13/2^+ \to 9/2^+$		
566.8	9257.3	16(2)	$(51/2^-) \to (49/2^-)$	0.46(5)	$M1 + E2$
574.4	1293.5		$17/2^- \to 15/2^-$	0.45(6)	$M1 + E2$
580.8	6374.2	34(5)	$39/2^- \to 37/2^-$	0.58(6)	$M1 + E2$
582.7	10489.3	9(1)	$(55/2^-) \to (53/2^-)$		
591.4	8954.8	33(4)	$49/2^- \to 47/2^-$	0.97(9)	$M1 + E2$
591.5	2821.8		$23/2^+ \to 19/2^+$		
602.3	7257.2	26(3)	$43/2^- \to 41/2^-$	0.82(9)	$M1 + E2$
607.4	7084.2	207(24)	$43/2^+ \to 41/2^+$	0.58(6)	$M1 + E2$
607.5	8224.3	25(3)	$47/2^- \to 45/2^-$	0.60(6)	$M1 + E2$
607.7	1269.6		$15/2^- \to 13/2^-$	0.61(6)	$M1 + E2$
(608.8)	3559.7		$27/2^+ \to 25/2^-$		
613.7	877.0		$13/2^- \to 11/2^-$	0.90(10)	$M1 + E2$
614.6	8690.0		$(49/2^-) \to 47/2^-$		
616.6	1335.3	1000	$19/2^- \to 15/2^-$	1.46(11)	E2
617.5	1953.1		$19/2^- \to 19/2^-$		
619.0	1553.5		$15/2^+ \to 11/2^+$		
629.9	1397.4		$15/2^+ \to 11/2^+$	1.34(14)	$E2$
631.5	11720.5	15(2)	$61/2^- \to 59/2^-$	0.63(7)	$M1 + E2$
631.6	1293.5		$17/2^- \to 13/2^-$	1.31(5)	$E2$
633.1	11808.8	48(6)	$(61/2^+) \to (59/2^+)$	0.73(7)	$M1 + E2$
644.6	1521.6		$17/2^- \to 13/2^-$		
649.3	9905.7	10(2)	$(53/2^-) \to (51/2^-)$		
651.7	2882.4		$23/2^+ \to 19/2^+$	1.37(14)	$E2$
655.1	6789.2	15(2)	$41/2^- \to 39/2^-$		
656.8	3478.6	139(18)	$27/2^+ \to 23/2^+$	1.37(11)	$E2$
669.8	4018.9		$29/2^+ \to 27/2^+$	0.40(5)	$M1 + E2$
670.1	9124.1	114(13)	$51/2^+ \to 49/2^+$	0.62(7)	$M1 + E2$
671.8	3168.7	253(31)	$25/2^+ \to 21/2^+$		
674.7	11720.5	8(1)	$61/2^- \to 57/2^-$		
675.8	1757.4		$17/2^+ \to 13/2^+$		
676.5	2230.0		$19/2^+ \to 15/2^+$		
677.3	3559.7	27(4)	$27/2^+ \to 23/2^+$	1.70(21)	$E2$
679.7	2769.2		$23/2^- \to 23/2^-$	0.44(5)	$M1 + E2$
683.5	1953.1		$19/2^- \to 15/2^-$	1.53(14)	$E2$
684.6	9809.5	6(1)	$(53/2^+) \to 51/2^+$		

TABLE I. (*Continued.*)

Energy E_γ (keV)[a]	Initial level energy E_i (keV)[b]	Intensity I_γ [c]	Spin assignment $I_i^\pi \to I_f^\pi$	Intensity ratio R_θ	Multipolarity assignment
685.6	11175.6	3(1)	$(57/2^-) \to (55/2^-)$		
695.6	3905.0	7(1)	$29/2^+ \to 25/2^+$	1.78(21)	$E2$
700.9	4608.5	182(21)	$31/2^- \to 27/2^-$	1.74(20)	$E2$
703.4	8693.5	9(1)	$49/2^+ \to 47/2^+$		
707.6	8189.4		$47/2^+ \to 45/2^+$	0.59(7)	$M1 + E2$
709.7	2821.8	168(22)	$23/2^+ \to 19/2^+$	1.67(18)	$E2$
710.7	5337.4	23(4)	$35/2^- \to 33/2^+$		
712.1	7969.8	14(2)	$45/2^- \to 43/2^-$	0.69(7)	$M1 + E2$
712.2	7990.6		$47/2^+ \to 43/2^+$		
712.4	3209.4	79(10)	$25/2^+ \to 21/2^+$	1.53(16)	$E2$
714.7	2112.1		$19/2^+ \to 15/2^+$	1.30(15)	$E2$
719.2	6789.2	34(5)	$41/2^- \to 37/2^-$	1.26(14)	$E2$
724.8	4879.6	6(1)	$33/2^+ \to 31/2^+$		
726.9	2062.0		$21/2^- \to 19/2^-$		
728.9	5337.4	170(20)	$35/2^- \to 31/2^-$	1.40(15)	$E2$
732.7	2821.8		$23/2^+ \to 23/2^-$		
733.6	2963.6		$23/2^+ \to 19/2^+$	1.69(24)	$E2$
734.3	4212.9	123(16)	$31/2^+ \to 27/2^+$	1.30(16)	$E2$
735.7	1397.4		$15/2^+ \to 13/2^-$		
737.3	8954.8	55(7)	$49/2^- \to 47/2^-$	0.82(11)	$M1 + E2$
738.9	3907.6	214(29)	$27/2^- \to 25/2^+$	0.77(13)	$E1$
739.6	2497.0	119(15)	$21/2^+ \to 17/2^+$	1.33(17)	$E2$
743.0	5026.3	71(9)	$33/2^- \to 29/2^-$	1.71(19)	$E2$
753.8	2089.1	875(81)	$23/2^- \to 19/2^-$	1.43(15)	$E2$
753.8	5687.1		$35/2^- \to (33/2^-)$		
755.1	4608.5		$31/2^- \to (27/2^-)$		
755.3	10889.9		$57/2^- \to 55/2^-$		
757.0	5793.4	48(6)	$37/2^- \to 35/2^+$		
762.7	2284.3		$21/2^- \to 17/2^-$	1.38(17)	$E2$
763.9	2990.9		$27/2^- \to (23/2^-)$		
765.9	4325.6	31(4)	$31/2^+ \to 27/2^+$	1.35(24)	$E2$
766.5	5793.4	51(6)	$37/2^- \to 33/2^-$	1.70(19)	$E2$
768.5	2062.0		$21/2^- \to 17/2^-$	1.56(17)	$E2$
770.3	2882.4	62(8)	$23/2^+ \to 19/2^+$	1.41(16)	$E2$
777.7	6464.6		$39/2^- \to 35/2^-$	1.20(15)	$E2$
778.3	10134.7	127(14)	$55/2^- \to 53/2^-$	0.65(8)	$M1 + E2$
780.2	9904.8	30(5)	$- \to 51/2^+$		
788.6	6374.2		$39/2^- \to 35/2^-$	1.26(16)	$E2$
788.7	4608.5	26(4)	$31/2^- \to 29/2^+$	0.95(18)	$E1$
796.0	6133.2	132(15)	$39/2^- \to 35/2^-$	1.40(15)	$E2$
802.8	1521.6		$17/2^- \to 15/2^-$		
806.3[d,e]	4155.4	439(52)	$31/2^+ \to 27/2^+$		
807.4[d,e,f]	4627.6		$33/2^+ \to 29/2^+$		
816.1	2769.2	264(29)	$23/2^- \to 19/2^-$	1.31(15)	$E2$
818.6	1081.6		$13/2^+ \to 11/2^-$		
819.4	4724.4	18(3)	$33/2^+ \to 29/2^+$	1.88(27)	$E2$
819.4	2112.1		$19/2^+ \to 17/2^-$		
820.0	2882.4		$23/2^+ \to 21/2^-$		
830.6	4934.0	19(2)	$(33/2^-) \to 29/2^-$		
830.6	11720.5	30(3)	$61/2^- \to 57/2^-$	1.54(19)	$E2$
848.7	5915.4	9(1)	$39/2^+ \to 35/2^+$		
850.5	4018.9	40(8)	$29/2^+ \to 25/2^+$	1.31(18)	$E2$
853.3	5066.2	105(13)	$35/2^+ \to 31/2^+$	1.46(19)	$E2$
858.6	5213.5		$(35/2^-) \to (31/2^-)$		
861.1	2950.6		$25/2^- \to 23/2^-$		M1
861.3	4879.6	54(9)	$33/2^+ \to 29/2^+$	1.68(24)	$E2$
861.5	6654.9	33(4)	$41/2^- \to 37/2^-$	1.69(21)	$E2$

TABLE I. (*Continued.*)

Energy E_γ (keV)[a]	Initial level energy E_i (keV)[b]	Intensity I_γ [c]	Spin assignment $I_i^\pi \rightarrow I_f^\pi$	Intensity ratio R_θ	Multipolarity assignment
862.1	3853.7		$(27/2^-) \rightarrow 27/2^-$		
868.2	3152.5	134(15)	$25/2^- \rightarrow 21/2^-$	1.60(22)	$E2$
871.1	5026.3		$33/2^- \rightarrow 31/2^+$		
875.3	2963.6		$23/2^+ \rightarrow 23/2^-$		
875.8	7990.6		$47/2^+ \rightarrow 43/2^+$		
875.9	2965.0	409(45)	$27/2^- \rightarrow 23/2^-$	1.49(18)	$E2$
879.2[d,e]	5915.4	734(88)	$39/2^+ \rightarrow 35/2^+$		
880.8[d,e]	5036.2		$35/2^+ \rightarrow 31/2^+$		
882.2	5207.8	25(4)	$35/2^+ \rightarrow 31/2^+$	1.40(20)	$E2$
883.7	7257.2		$43/2^- \rightarrow 39/2^-$		
887.8	3853.7		$(27/2^-) \rightarrow 27/2^-$		
888.6	2950.6	141(17)	$25/2^- \rightarrow 21/2^-$	1.89(27)	$E2$
891.8	5519.1	100(12)	$37/2^+ \rightarrow 33/2^+$	1.29(18)	$E2$
901.9	2990.9		$27/2^- \rightarrow 23/2^-$	1.84(25)	$E2$
906.4	7990.6	113(14)	$47/2^+ \rightarrow 43/2^+$	1.43(18)	$E2$
910.9	11045.6	20(2)	$57/2^- \rightarrow 55/2^-$	0.83(12)	$M1 + E2$
916.7	3907.6	142(17)	$27/2^- \rightarrow 27/2^-$		
919.2	7084.2	5(1)	$43/2^+ \rightarrow 39/2^+$		
926.4	5650.8	9(2)	$37/2^+ \rightarrow 33/2^+$	1.71(21)	$E2$
933.1	7066.3	68(8)	$43/2^- \rightarrow 39/2^-$	1.48(19)	$E2$
934.2	4283.3		$29/2^- \rightarrow 27/2^+$	0.74(9)	$E1$
934.9	9124.1	29(4)	$51/2^+ \rightarrow 47/2^+$	1.23(18)	$E2$
936.1	2230.0		$19/2^+ \rightarrow 17/2^-$		
939.9	3905.0	4(1)	$29/2^+ \rightarrow 27/2^-$		
941.0	13432.6	14(2)	$67/2^- \rightarrow 63/2^-$	1.45(19)	$E2$
942.6	3907.6	300(35)	$27/2^- \rightarrow 27/2^-$	1.08(12)	$M1 + E2$
944.3	10068.4	98(12)	$55/2^+ \rightarrow 51/2^+$	1.53(23)	$E2$
948.9	2284.3		$21/2^- \rightarrow 19/2^-$	1.08(15)	$M1 + E2$
950.9	4103.4	86(10)	$29/2^- \rightarrow 25/2^-$	1.48(22)	$E2$
954.6	11089.3	40(5)	$59/2^- \rightarrow 55/2^-$	1.70(23)	$E2$
957.7	6165.5	15(2)	$39/2^+ \rightarrow 35/2^+$	1.48(22)	$E2$
958.1	6476.8	89(11)	$41/2^+ \rightarrow 37/2^+$	1.40(21)	$E2$
960.6	6070.0		$37/2^- \rightarrow 33/2^-$	1.62(24)	$E2$
960.8[e]	8217.8	42(6)	$47/2^- \rightarrow 43/2^-$		
961.3	5064.3		$(33/2^-) \rightarrow 29/2^-$		
962.5[e]	7616.8		$45/2^- \rightarrow 41/2^-$	1.62(21)	$E2$
965.4	9418.7	65(8)	$53/2^+ \rightarrow 49/2^+$	1.63(21)	$E2$
966.7	8224.3		$47/2^- \rightarrow 43/2^-$		
967.6	6033.8	117(15)	$39/2^+ \rightarrow 35/2^+$	1.54(20)	$E2$
971.9	8453.3	112(13)	$49/2^+ \rightarrow 45/2^+$	1.76(23)	$E2$
985.0	8954.8		$49/2^- \rightarrow 45/2^-$		
985.8	3950.8	279(30)	$31/2^- \rightarrow 27/2^-$	1.52(15)	$E2$
1000.1	6418.1	16(2)	$39/2^- \rightarrow 35/2^-$	1.34(16)	$E2$
1004.7	7481.4	102(12)	$45/2^+ \rightarrow 41/2^+$	1.59(22)	$E2$
1005.3[d,e]	6048.6	118(15)	$(37/2^-) \rightarrow (33/2^-)$		
1005.4[d,e]	3956.0		$(29/2^-) \rightarrow 25/2^-$		
1005.7	6070.0	35(4)	$37/2^- \rightarrow (33/2^-)$		
1008.4	8074.7	54(7)	$47/2^- \rightarrow 43/2^-$	1.32(20)	$E2$
1027.3	6070.0		$37/2^- \rightarrow (33/2^-)$		
1029.6	11098.0	21(4)	$57/2^+ \rightarrow 55/2^+$	0.58(10)	$M1 + E2$
1032.8	6683.6	7(1)	$41/2^+ \rightarrow 37/2^+$	1.26(13)	$E2$
1035.6	6045.5	129(14)	$39/2^- \rightarrow 35/2^-$	1.37(15)	$E2$
1038.3	1757.4		$17/2^+ \rightarrow 15/2^-$	0.85(11)	$E1$
1048.8	12146.8	12(2)	$61/2^+ \rightarrow 57/2^+$	1.58(22)	$E2$
1050.2	7084.2	36(4)	$43/2^+ \rightarrow 39/2^+$	1.51(21)	$E2$
1059.1[e]	5009.9	239(28)	$35/2^- \rightarrow 31/2^-$	1.83(24)	$E2$
1060.9[e]	7106.4		$43/2^- \rightarrow 39/2^-$	1.55(20)	$E2$

TABLE I. (*Continued.*)

Energy E_γ (keV)[a]	Initial level energy E_i (keV)[b]	Intensity I_γ [c]	Spin assignment $I_i^\pi \to I_f^\pi$	Intensity ratio R_θ	Multipolarity assignment
1062.7	3152.5		$25/2^- \to 23/2^-$		
1064.7	11133.1	15(3)	$- \to 55/2^+$		
1073.2	8690.0	18(3)	$(49/2^-) \to 45/2^-$		
1079.6	3168.7	407(45)	$25/2^+ \to 23/2^-$	0.80(9)	$E1$
1080.7	7114.5	58(8)	$43/2^+ \to 39/2^+$	1.29(22)	$E2$
1084.5	3853.7	47(6)	$(27/2^-) \to 23/2^-$		
1087.3	5043.3	34(5)	$(33/2^-) \to (29/2^-)$		
1105.4	8189.4		$47/2^+ \to 43/2^+$	1.66(28)	$E2$
1107.3	11175.7	41(6)	$(59/2^+) \to 55/2^+$		
1111.4	8217.8	76(8)	$47/2^- \to 43/2^-$	1.76(23)	$E2$
1113.7	7279.2	10(2)	$43/2^+ \to 39/2^+$	1.22(22)	$E2$
1115.8	14553.6	7(1)	$(69/2^-) \to 65/2^-$		
1118.1	8224.3	21(3)	$47/2^- \to 43/2^-$		
1120.8	3209.4	34(4)	$25/2^+ \to 23/2^-$		
1123.7	7807.3		$45/2^+ \to 41/2^+$	1.87(34)	$E2$
(1126.9)	12216.2	3(1)	$- \to 59/2^-$		
1128.1	2422.1		$19/2^+ \to 17/2^-$	0.80(9)	$E1$
1133.3	9124.1	18(2)	$51/2^+ \to 47/2^+$	1.67(21)	$E2$
1137.1	12857.6		$- \to 61/2^-$		
1138.3	3907.6	147(18)	$27/2^- \to 23/2^-$	1.60(21)	$E2$
1141.8[d,e]	10707.7	8(2)	$(55/2^+) \to (51/2^+)$		
1143.0[d,e]	11850.7		$(59/2^+) \to (55/2^+)$		
1146.5	12235.8	8(1)	$63/2^- \to 59/2^-$	1.86(27)	$E2$
1152.0	9376.3		$(51/2^-) \to 47/2^-$		
1153.2	5109.4		$33/2^- \to (29/2^-)$		
1156.4	7840.0		$- \to 41/2^+$		
1160.9	2497.0	68(9)	$21/2^+ \to 19/2^-$		
1162.9	12296.0	14(3)	$\to$		
1166.9[e]	9464.8	10(2)	$- \to (47/2^+)$		
1168.8	7084.2	85(10)	$43/2^+ \to 39/2^+$	1.47(19)	$E2$
1169.2[e]	10634.0		$\to$		
1169.8	8449.0	3(1)	$(47/2^+) \to 43/2^+$		
1174.5	8954.8		$49/2^- \to 45/2^-$		
1178.2	10596.9	11(2)	$(57/2^+) \to 53/2^+$		
1180.6	7969.8	58(7)	$45/2^- \to 41/2^-$	1.22(12)	$E2$
1182.2	9257.3	26(4)	$(51/2^-) \to 47/2^-$		
1183.4	8297.9	28(4)	$(47/2^+) \to 43/2^+$		
1194.4	8974.7		$(49/2^-) \to 45/2^-$		
1195.0	10613.7	11(2)	$57/2^+ \to 53/2^+$	1.47(22)	$E2$
1196.0	13432.6	6(1)	$67/2^- \to 63/2^-$		
1197.4	10573.7		$(55/2^-) \to (51/2^-)$		
1202.0	13437.8		$65/2^- \to 63/2^-$	0.28(8)	$M1 + E2$
1204.6	9422.4	35(4)	$51/2^- \to 47/2^-$	1.23(18)	$E2$
1211.3	11808.8		$(61/2^+) \to (57/2^+)$		
1212.7	8693.5	17(2)	$49/2^+ \to 45/2^+$		
1215.7	9905.7	13(2)	$(53/2^-) \to (49/2^-)$		
1216.2	12039.8	16(2)	$61/2^+ \to 57/2^+$	1.73(29)	$E2$
(1222.1)	13437.8		$65/2^- \to -$		
1225.5	5328.9		$(33/2^-) \to 29/2^-$		
1228.3	11133.1		$\to$		
1232.0	10489.3	14(3)	$(55/2^-) \to (51/2^-)$		
1234.2	12322.8		$- \to 59/2^-$		
1251.9	6464.6		$39/2^- \to (35/2^-)$		
1256.6[e]	8363.4	29(4)	$47/2^- \to 43/2^-$		
1257.0[e]	10679.4		$55/2^- \to 51/2^-$	1.26(20)	$E2$
1262.5	5213.5		$(35/2^-) \to 31/2^-$		
(1264.0)	11898.0		$\to$		

TABLE I. (*Continued.*)

Energy E_γ (keV)[a]	Initial level energy E_i (keV)[b]	Intensity I_γ[c]	Spin assignment $I_i^\pi \rightarrow I_f^\pi$	Intensity ratio R_θ	Multipolarity assignment
1268.0	9565.9	9(2)	$(51/2^+) \rightarrow (47/2^+)$		
1269.9	11175.6	6(1)	$(57/2^-) \rightarrow (53/2^-)$		
1288.5	11098.0	6(1)	$57/2^+ \rightarrow (53/2^+)$		
1292.4	9590.3		$- \rightarrow (47/2^+)$		
1311.6	14485.1	20(3)	$- \rightarrow (65/2^+)$		
1318.9	11998.3	14(2)	$(59/2^-) \rightarrow 55/2^-$		
1327.2	14759.8	10(2)	$69/2^- \rightarrow 67/2^-$	0.24(7)	$M1 + E2$
1329.5	5285.5		$(33/2^-) \rightarrow (29/2^-)$		
1348.2	14521.7	27(3)	$- \rightarrow (65/2^+)$		
1352.4	2688.4		$21/2^+ \rightarrow 19/2^-$		
1355.3	9809.5	11(2)	$(53/2^+) \rightarrow 49/2^+$		
1364.7	13173.5	58(6)	$(65/2^+) \rightarrow (61/2^+)$		
1372.4	11440.8		$- \rightarrow 55/2^+$		
1389.9	4354.9		$(31/2^-) \rightarrow 27/2^-$		
1402.3	12491.6	14(2)	$63/2^- \rightarrow 59/2^-$	1.78(28)	$E2$
1404.9	10823.6	33(5)	$57/2^+ \rightarrow 53/2^+$	1.84(30)	$E2$
1408.2	6418.1	11(2)	$39/2^- \rightarrow 35/2^-$		
1454.7	6464.6	31(7)	$39/2^- \rightarrow 35/2^-$	1.76(18)	$E2$
1466.6	5418.0		$35/2^- \rightarrow 31/2^-$		
1480.5	12921.3	7(2)	$\rightarrow$		
1534.0	10889.9	9(2)	$57/2^- \rightarrow 53/2^-$		
1764.1	3853.7		$(27/2^-) \rightarrow 23/2^-$		
1818.9	3907.6	73(15)	$27/2^- \rightarrow 23/2^-$		

[a]The uncertainties in γ-ray energies lies between 0.2 and 1.0 keV depending on intensity.

[b]The energy levels have been determined using the centroid of the most intense transition decaying from the level. The uncertainties of the level energies lie between 0.2 and 1.0 keV.

[c]Intensities for γ rays are normalized to that of 616.6 keV transition, with $I_\gamma = 1000$.

[d]Measurement of angular distribution ratio R_θ was not possible due to the presence of γ rays of overlapping energy.

[e]The quoted intensity is the combined value for γ rays of overlapping energies.

[f]The energy of γ ray could not be measured exactly due to the presence of multiple γ rays of similar energy.

been observed. These transitions confirm the placement of the levels and provide restrictions on possible spins. The 684 and 816 keV γ rays of band 4 have been identified as $E2$ transitions [$R_\theta = 1.53(14)$ and $1.31(15)$, respectively].

A new cascade of transitions, labeled band 6, has been found to feed band 5 at higher spin. Some of the decay transitions from the lower part of the band; e.g., the 1455, 1262, and 1390 keV transitions decaying to band 9, were reported in previous work [29] and have been confirmed. The band structure is irregular and exhibits a fragmented decay pattern to several sequences. Intense γ rays of energies 325, 1181, 985, 778, and 402 keV were observed in coincidence with the 1455 keV transition and a list comprising γ rays from the lower portion of the yrast band, band 9. The spins of the levels in band 6 could be established through the 1455 and 325 keV transitions of quadrupole and dipole character, respectively. The assignments are further supported by the dipole nature of the 712 and 737 keV transitions linking band 6 to bands 3 and 9, respectively (see Table I). Bands 7 and 8 are extensions of band 6 to higher spin and, together with band 6, most likely represent noncollective excitations. The placements of the levels are justified by several linking transitions between these states as well as to other bands. With the tentative assignment of a spin to the highest level observed

in this work, band 7 extends up to a spin of 69/2. The newly added γ-ray transitions are visible in Fig. 5.

The yrast band 9 has been extended to an $I^\pi = 59/2^-$ state above the previously known $51/2^-$ level with the addition of γ rays of 1257 and 1319 keV. Similarly, band 10 has been extended to $I = 37/2$ by adding another 1005 keV γ ray on top of the band. A cascade of 961 and 1153 keV transitions from band 6 has been observed to feed band 10 at the 29/2 level.

C. Bands 11, 12, 13, and their extensions

Band 11 was established in previous work and was assigned positive parity [28,29]. Several deexcitation paths in and out of the band have been observed in the present work.

Bands 12 and 13 were previously reported by Schmidt *et al.* [29] up to a tentative spin of $(53/2^+)$. In the present work, these bands have been extended with the addition of five (1178, 1211, 1365, 1348, 1312 keV) and three (1133, 944, 1107 keV) new γ rays in bands 12 and 13, respectively. The angular distribution ratio of 1.53(23) could be measured only for the 944 keV γ ray confirming its stretched $E2$ character. For the other transitions, an $E2$ multipolarity has been assumed in view of the apparent rotational character of
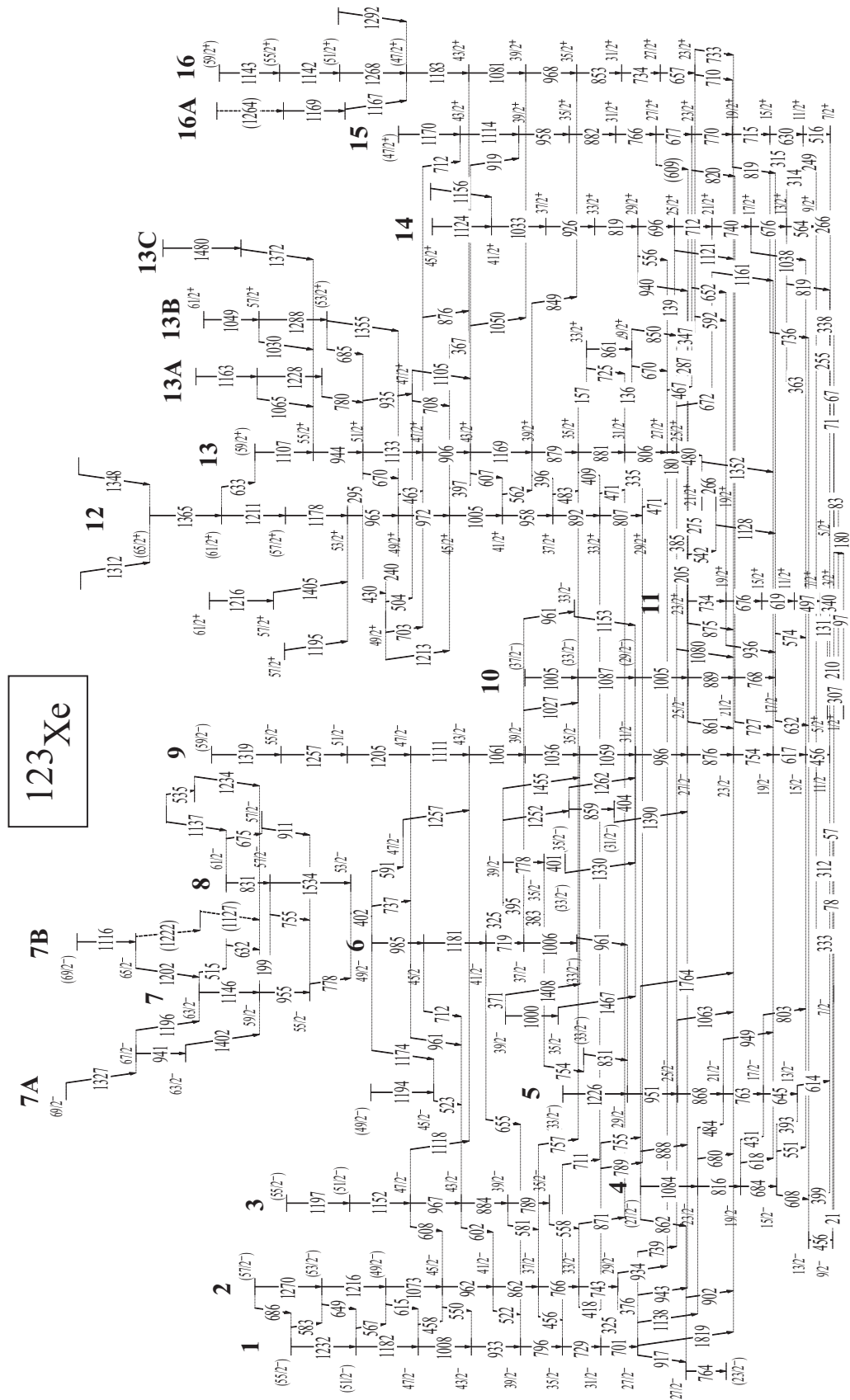
FIG. 2. The partial level scheme of ^{123}Xe based on experiments in the present work and in Refs. [28–30].
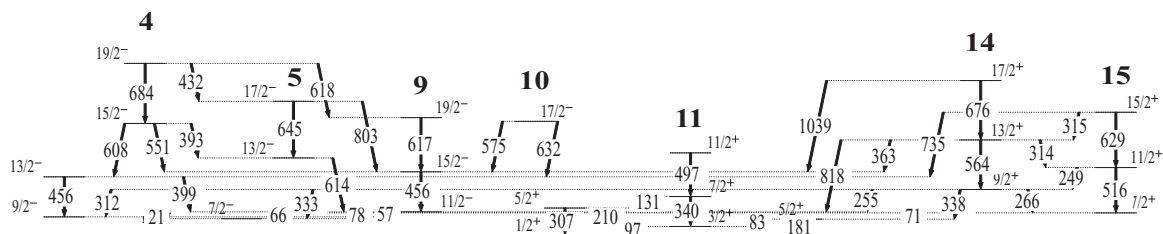
FIG. 3. Low-energy levels of ^{123}Xe displayed in expanded energy scale. The levels have been taken from Refs. [28–30,33].

the sequences. At higher spin, the angular distribution ratio measured for the 633 keV transition indicates its dipole nature with some $E2$ mixing.

The three cascades labeled 13A, 13B, and 13C, each consisting of two or three transitions, have been observed to feed band 13 at higher spin. Spins could not be assigned to the levels of 13A and 13C due to poor statistics. A cluster of decay transitions has been observed around spin 51/2 of band 13; these are visible in a coincidence spectrum gated by transitions of bands 12 and 13; see Fig. 6(a). Another cluster of transitions connecting levels of bands 13 and 14 is observed around spin 35/2. These decay transitions indicate strong mixing of the levels involved.

D. Bands 14, 15, 16, and their extensions

Bands 14 and 15 have been considerably extended in the current work. Band 14, which was earlier known to a spin of 29/2, has been extended to $I = 45/2$ with the addition of the 819, 926, 1033, 1124, and 1156 keV γ rays [see Fig. 7(a)]. Similarly, band 15 has been extended to spin (47/2) with the addition of six new γ rays [see Fig. 7(b)]. Several decay transitions of $E1$ character were reported between bands 14, 15, and bands 9, 10 [29]. A few more such transitions have been added at lower energy. Several decay transitions from band 13 to band 15 have also been observed at higher spin.

Band 16 was established up to spin 47/2 in previous work [29]. Here, the band has been extended to spin (59/2). Furthermore, a new branch, 16A, has been found to feed band 16 at spin 47/2. The angular distribution ratio of the new transitions could not be measured accurately due to poor statistics and, hence, spin values could not be assigned to the levels. A new decay transition of 733 keV has been observed from the $23/2^+$ state of band 16 to the $23/2^-$ level of band 9. At higher spin, decay transitions of 876, 367, 1050, and
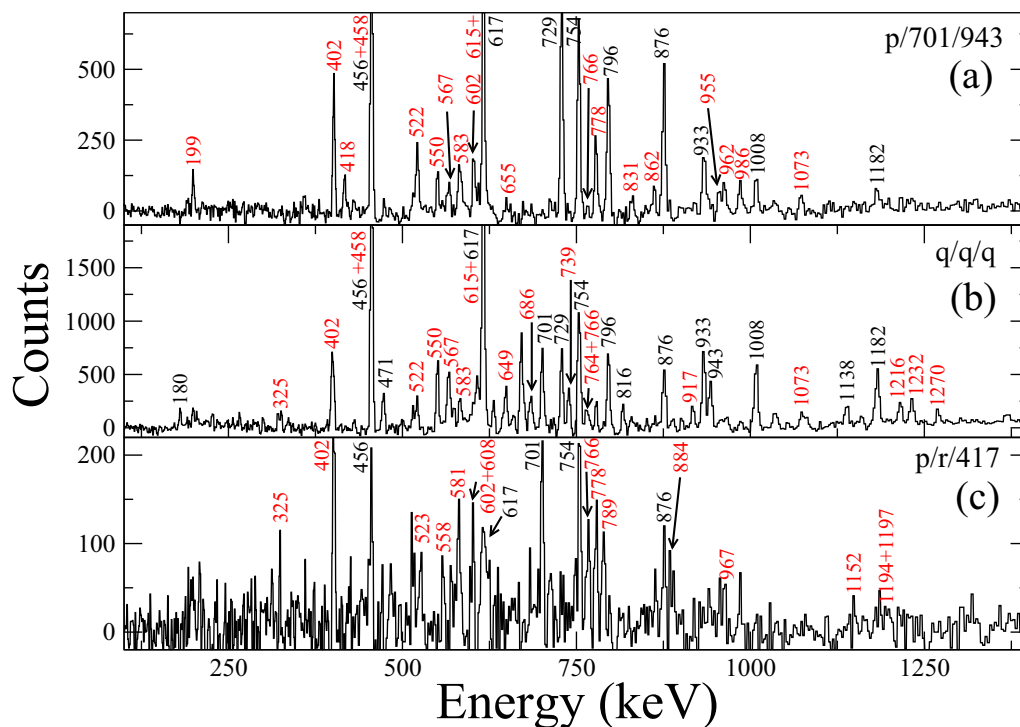
FIG. 4. Background-subtracted summed triple-gated γ-ray coincidence spectra. (a) Spectrum obtained with gates on a list p of four transitions of 456, 617, 754, and 876 keV of band 9, and on the 701 and 943 keV transitions at the bottom of band 1. (b) Quadruple coincidences of list q, which contains the 701, 729, 796, 933, and 1008 keV transitions of bands 1 and 2. (c) Coincidences of lists p and r and of the 418 keV transition, where list r contains the 558, 789, and 884 keV transitions of band 3. The peaks marked in red are the newly observed transitions.
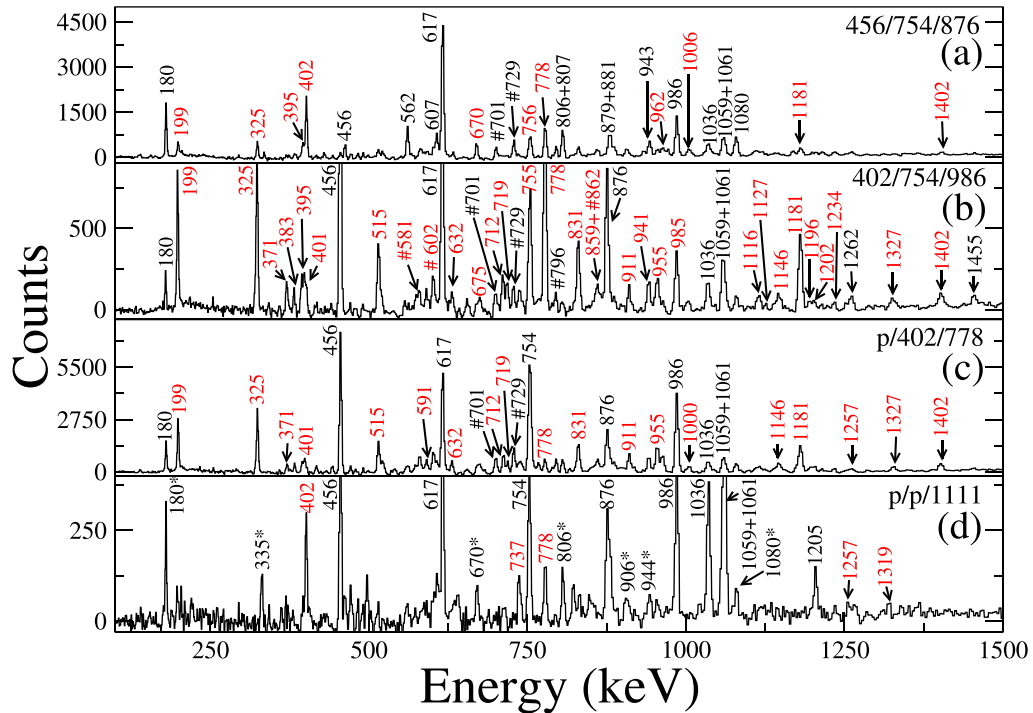
FIG. 5. Background-subtracted summed triple-gated γ-ray coincidence spectra. (a) Spectrum obtained with triple gates on 456, 754, and 876 keV transitions. The transitions of band 6 and its decay-out transitions are displayed. (b) The presence of second 401, 755, and 985 keV γ rays can be seen in spectrum with triple gates on 402, 754, and 986 keV. (c) Quadruple coincidence of list p of 456, 617, 754, and 876 keV transitions of band 9, and the 402 and 778 keV transitions. The transitions of bands 7 and 8 can be seen in this spectrum. (d) Quadruple-coincidence spectrum with two gates on γ rays from list p, and the 1111 keV transition of band 9. The new transitions of band 9 and the 737 keV transition linking bands 7 and 8 to band 9 are displayed. The γ rays marked by # belong to bands 1–3. The transitions marked by * are from bands 12 and 13 of ^{123}Xe. The new transitions are marked in red.

849 keV have been observed from band 13. These transitions are seen in Fig. 7(c).

IV. DISCUSSION

The Xe nuclei in the mass 125 region are well known for possessing a variety of shapes as a function of angular momentum [1,2,12,27]. In these nuclei, the neutron Fermi surface lies in the upper region of the $N = 50$–82 shell (see Fig. 1) and a shape change from a prolate to an oblate one involves a major change in occupancy of the $h_{11/2}$ orbitals. Hence, significant changes in the characteristics of the bands can be expected. Theoretical calculations in Ref. [1] predict that coexisting minima are present in ^{123}Xe with triaxial shapes playing a significant role.

The low- and medium-spin states of ^{123}Xe were known from previous work [28,29] and configurations to the bands were assigned on the basis of a core-quasiparticle coupling model. Also, tentative configurations were suggested for some of the bands on the basis of band-crossing frequencies and alignment gains. In the following, the bands are compared with those observed in neighboring nuclei and possible configurations are qualitatively discussed. For medium- and high-spin states, the results from the configuration-dependent cranked Nilsson-Strutinsky (CNS) formalism [4,35,36] are compared with the data.

It is instructive to plot the observed bands in ^{123}Xe relative to the rotating liquid drop energy; see Fig. 8. The figure suggests the presence of regular deformed bands up to $I \approx 41/2$; a mixture of such bands and more irregular sequences in the $I = 41/2$–61/2 spin range as well as the presence of a few bands or states lying relatively low in energy for spin values just above $I = 61/2$. This suggests small collectivity for $I > 41/2$ with some configurations reaching or approaching termination for $I = 61/2$–71/2. This is in line with the interpretation of the level schemes for neighboring nuclei, see e.g., Refs. [7,18,19,25].

A. The cranked Nilsson-Strutinsky formalism

The medium- and high-spin states of various nuclei in the $A \simeq 125$ mass region [7,9,18,19] have been successfully interpreted by using the cranked Nilsson-Strutinsky (CNS) formalism [4,35,36]. In this model, the orbitals in each $\mathcal{N}$ major shell are grouped into high- and low-j orbits, respectively. A further division according to signature $\alpha = 1/2$ and $\alpha = -1/2$ is made. The configurations are then labeled by the number of particles or holes in each group. It should be noted that no distinction between the core and valence particles are made and all the $\mathcal{N}$ shells up to $\mathcal{N} = 8$ are treated on an equal footing. The configurations are labeled as
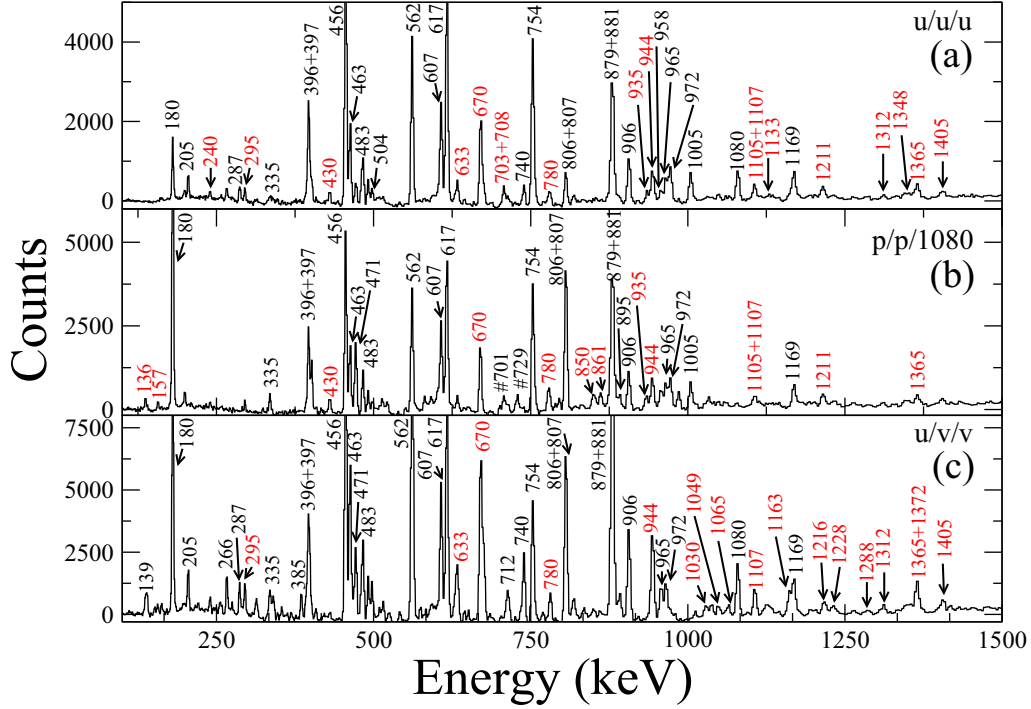
$$[p_1 p_2, n_1 n_2],$$

FIG. 6. Background-subtracted summed triple-gated γ-ray coincidence spectra. (a) Quadruple-coincidence spectrum with gates on list u, containing 1080, 180, 806, and 881 keV γ rays of bands 12 and 13. (b) Coincidence spectrum with two gates on transitions of list p containing 456, 617, 754, and 876 keV of band 9, and the 1080 keV transition. The decay-out transitions from band 13 can be noted. (c) Quadruple-coincidence spectrum with two gates on list v containing γ rays of 607, 463, 670, and 906 keV of bands 12 and 13, and a gate on list u. The transitions of bands 13A, 13B, and 13C are visible. The new transitions are marked in red.

where p_1 and p_2 are the number of protons in $d_{5/2}g_{7/2}$ (dg) and $h_{11/2}$ orbitals, respectively, whereas n_1, n_2 are the number of $\mathcal{N} = 4$ neutron holes and $h_{11/2}$ neutrons, respectively. If neutrons are excited to orbitals in the $h_{9/2}f_{7/2}$ (hf) and/or $i_{13/2}$ shells above the $N = 82$ gap, the configurations are specified as $[p_1p_2, n_1n_2(n_3n_4)]$, where n_3 and n_4 are the number of hf and $i_{13/2}$ particles, respectively. Furthermore, for an odd number of particles in some group, the signature is often specified by a subscript, "+" for $\alpha = 1/2$ and "−" for $\alpha = -1/2$, while if a signature is not specified, a configuration is fully defined by the number of high-j particles, $[p_2, n_2]$.

In the present calculations, the $A \simeq 110$ parameters, i.e., the κ and μ parameters defining the $l \cdot s$ and l^2 strengths of the oscillator potential, have been used [4]. The sum of the shell energy and the rotating liquid-drop energy is used to calculate the excitation energies. The rotating liquid-drop energy has been modeled according to the Lublin-Strasbourg drop model [37], while the rigid-body moments of inertia have been calculated with an $r_0 = 1.16$ fm radius parameter and an $a = 0.6$ fm diffuseness parameter [36]. As the energy of each configuration is minimized at each spin in the deformation space (ε_2, ε_4, γ), one can follow the development of collectivity as a function of angular momentum. Pairing correlations are not included in the CNS formalism and this implies that the results are pertinent at high spins, where pairing effects are negligible. However, in the recent work in the mass-125 region [7,9,16–20], it was established that the CNS model works quite well even in the intermediate-spin regions ($I >$

15) and it provides at least a qualitative understanding for lower-spin states; see, e.g., Ref. [38].

1. Valence-space orbitals

The CNS configurations which are expected to be low in energy in ^{123}Xe can be identified from Fig. 1, where the single-particle orbitals in the 50–82 shell are drawn at a prolate shape up to $\varepsilon_2 = 0.22$ and then as a function of rotational frequency at this deformation. Even though many configurations in ^{123}Xe appear to be triaxial, this diagram provides a general understanding of the j shells around the Fermi surface and of their occupation. The figure suggests that the ground-state configuration has the odd particle in the $\mathcal{N} = 4$ orbital [402]5/2 with six neutrons in $h_{11/2}$ orbitals. Other low-lying, positive-parity neutron configurations might be formed with the odd neutron in the [411]1/2 or the [404]7/2 orbital. Furthermore, the low-lying, negative-parity configurations are formed with either 7 or 5 $h_{11/2}$ neutrons. Note also that, for the low-spin yrast configurations, there are in total two or three holes in the [404]7/2 and the [402]5/2 orbitals; i.e., there are at least two holes in the $N = 64$ core. However, with increasing spin, the deformation generally becomes smaller and it might be advantageous to close the $N = 64$ core. Since the Fermi surface is in the middle of the $h_{11/2}$ shell, it is expected that, with increasing spin, it will be energetically favorable to occupy fewer $h_{11/2}$ orbitals. This tendency is, for example, illustrated in Fig. 12.11 of Ref. [3].
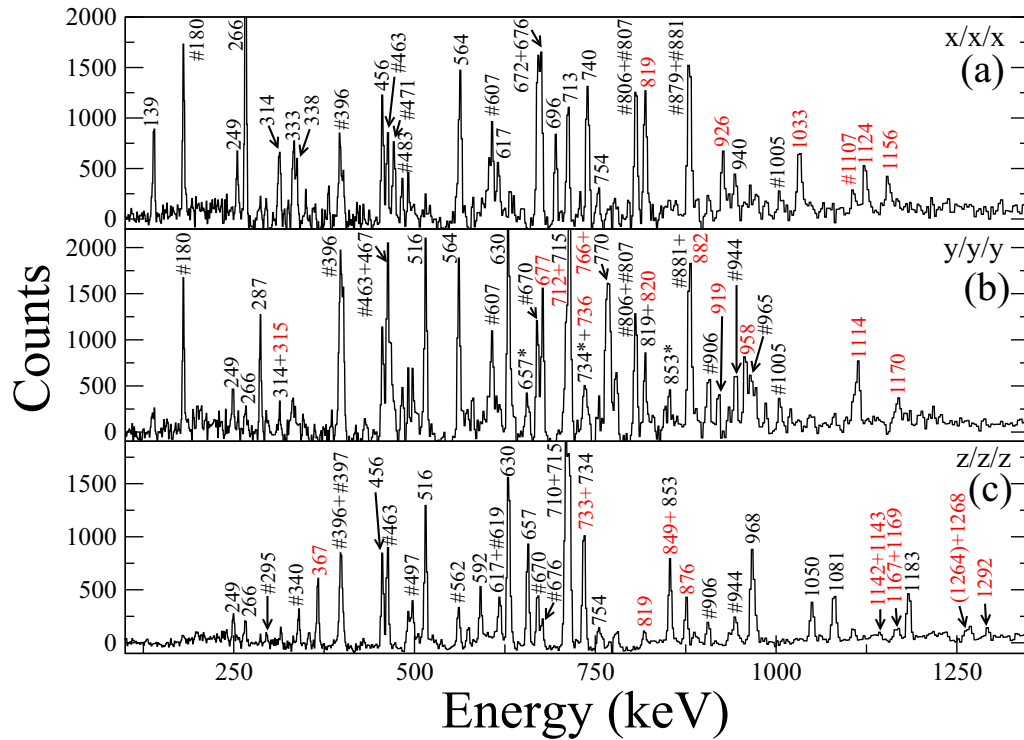
FIG. 7. Background-subtracted summed triple-gated γ-ray coincidence spectra. (a) Quadruple-coincidence spectrum on list x, which contains 564, 676, 740, 712, 696, 819, 926, and 1033 keV transitions of band 14. (b) Coincidence spectrum with triple gates on list y containing 516, 630, 715, 770, 677, 766, 882, and 958 keV transitions of band 15. (c) Coincidence spectrum with triple gates on list z containing transitions of 657, 734, 853, 968, and 1081 keV of band 16. The new interband links between bands 13 and 16 are also visible. The #-marked peaks depict transitions from bands 11–13. The γ-ray peaks marked by * are transitions from band 16 of ^{123}Xe. The new transitions are marked in red.

The protons occupy four orbitals above the $Z = 50$ gap. They all occupy dg orbitals in energetically favored low-spin states; see Fig. 1. With increasing spin, it is expected that it becomes energetically favorable to lift one proton to the $h_{11/2}$ shell. This shell is so high in energy that states with two $h_{11/2}$ protons are calculated to be located at a rather high excitation energy for low and intermediate spin values.

2. Favored aligned states

There is an analogy between the $A = 155$–160 region and the present $A = 125$ one that has been exploited previously; see, e.g., Refs. [7,13]. The protons in the heavier region fill the same orbitals above particle number 64 as the neutrons in the present region. In addition, there is a limited number of protons outside the $Z = 50$ gap in the present region in a similar way that there is a limited number of neutrons outside the $N = 82$ gap in the $A = 155$–160 region. The analogy suggests that favored terminating bands are formed from configurations with a closed ^{114}Sn core and that these will terminate when all spin vectors of the particles outside the core are aligned, which corresponds to $I \approx 63/2$ for ^{123}Xe. Bands of this type have been observed for several other nuclei in the $A = 125$ region [7,10,16–20].

The favored aligned configurations for $Z = 54$ and $N = 69$ are illustrated in sloping Fermi-surface diagrams [13] in Fig. 9, while low-lying terminating bands are drawn relative to the rotating liquid-drop energy in Fig. 10. For protons with four valence particles outside the $Z = 50$ core, straight-line Fermi surfaces are naturally drawn with one or two $h_{11/2}$ particles; i.e., for the configurations $(dg)^3(h_{11/2})^1$ and $(dg)^2(h_{11/2})^2$ with $I_{max} = 14$ and $I_{max} = 16$, respectively. For the neutrons, the most favored configuration is $(h_{11/2})^4(sd)^1$ with $I_{max} = 35/2$; see Fig. 9. Combining this neutron configuration with the two proton configurations results in bands terminating in the two most favored states in Fig. 10; the $63/2^-$ state of a [31,54] configuration and the $67/2^+$ level of a [22,54] configuration. There are other [31,54] and [22,54] configurations drawn in Fig. 10, terminating one spin unit lower, where either the third dg proton is placed in a $m_i = 3/2$ state instead of a $m_i = 5/2$ one or the sd ($s_{1/2}d_{3/2}$) neutron is placed in $m_i = 1/2$ instead of $m_i = 3/2$. Furthermore, configurations with the fifth valence neutron in the $m_i = 3/2$, $h_{11/2}$ state instead of the $m_i = 3/2$ one of sd character, [31,65] and [22,65], are also displayed in Fig. 10. With the present parameters, these alternative bands with negative neutron parity are less favored than [31,54] and [22,54], but with small changes in parameters, the situation could be reversed.

Starting from the configurations with a closed core, higher-spin terminating configurations can be formed with one or two neutrons excited across the $N = 64$ gap, as shown by the broken line Fermi surface in Fig. 9(b) for the one-neutron excitation. On the other hand, excitations over the larger proton gap at $Z = 50$ will not result in any energetically competitive
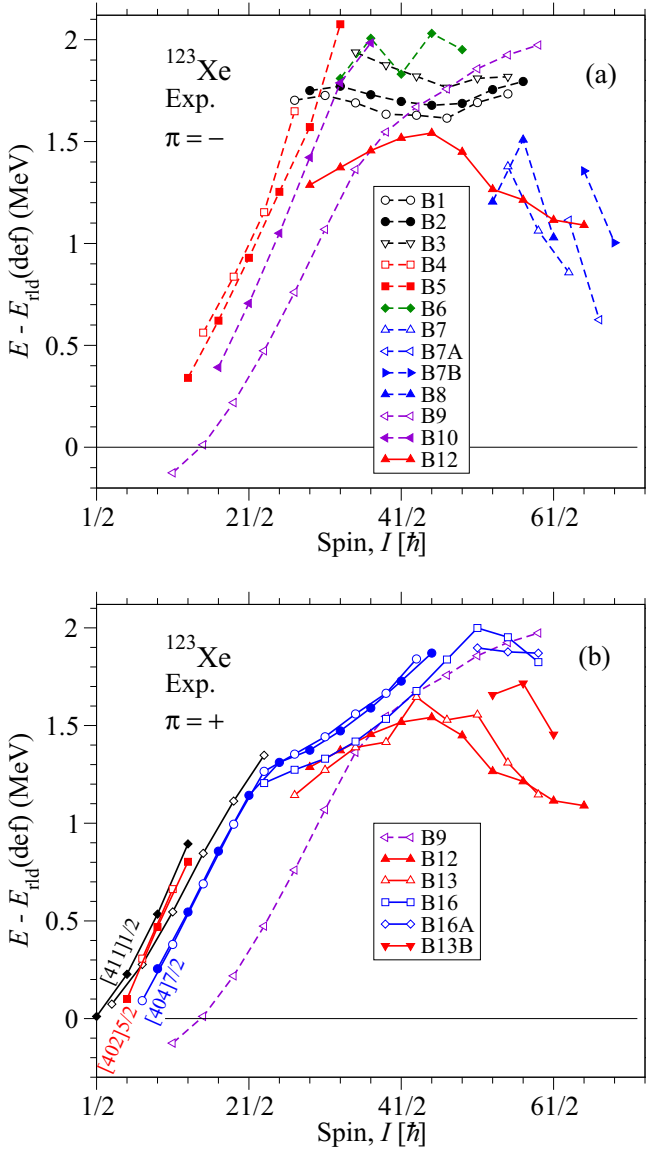
FIG. 8. The observed energy levels of (a) negative-parity bands and (b) positive-parity bands in ^{123}Xe plotted relative to the rotating liquid-drop energy. The positive-parity band 12 in panel (a) and negative-parity band 9 in panel (b) have been included for comparison. The low-spin positive-parity bands have been taken from Ref. [30] and are labeled by the asymptotic orbitals on which they are built. The [404]7/2 band is labeled 14, 15 in Fig. 2 and the $\alpha = -1/2$ branch of the [411]1/2 band is labeled 11. Positive-parity (negative-parity) bands are drawn by full (dashed) lines and closed (open) symbols are used for signature $\alpha = 1/2$ ($\alpha = -1/2$) states. This convention is used for all figures.

terminating configurations. The combination of the one-particle-one-hole (1p-1h) or 2p-2h neutron configurations with the closed core proton configurations leads to terminating states at higher spin, as shown in Fig. 10. Furthermore, favored noncollective states might also be formed with some spin vector anti-aligned. Especially, the $I = 53/2$ state of the [22,65] configuration stands out in Fig. 10. In this state, all the valence neutrons are in $h_{11/2}$ orbitals, but with one of these in the $m_i = -11/2$ orbital [see Fig. 9(b)], leading to a neutron
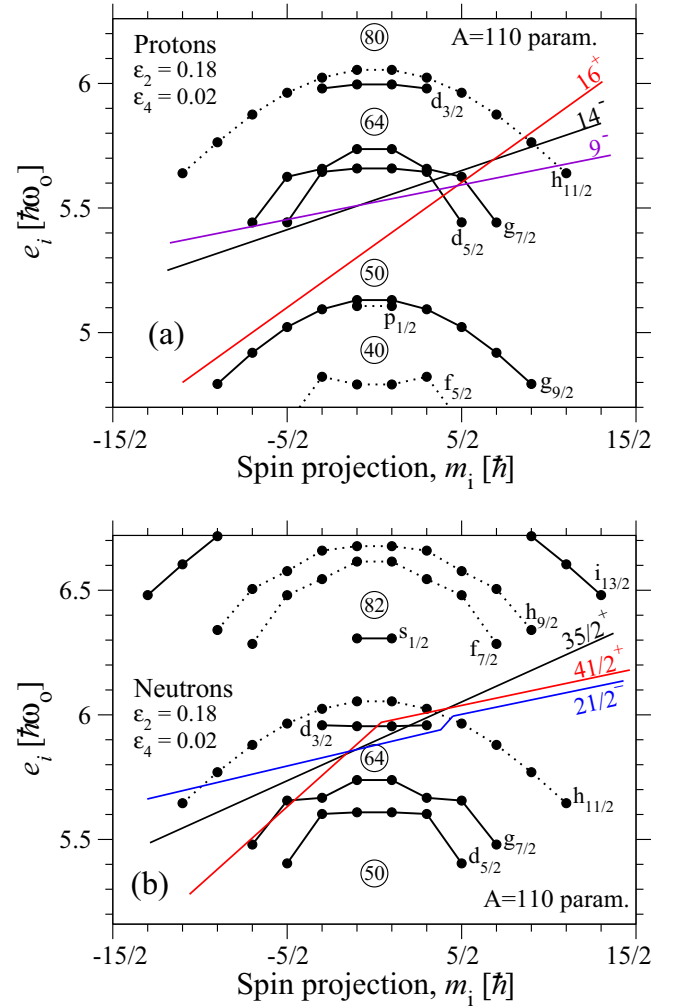
FIG. 9. Calculated single-particle energies e_i as a function of the spin-projection quantum number, m_i, calculated at $\varepsilon_2 = 0.18$, $\gamma = 60°$, and $\varepsilon_4 = 0.020$ (a) for protons and (b) for neutrons. Some low-lying aligned configurations are defined by "straight-line Fermi surfaces" [13], where the orbitals below the lines are occupied and the total spin is obtained as the sum of the projections m_i below the lines.

spin of $21/2^-$. Thus, a total spin of $53/2$ is obtained when combined with the proton spin of 16^+. Indeed, aligned states with this kind of anti-aligned spin vectors are calculated to be yrast for many spin values. They might be assigned to some states not placed in bands in the level scheme or might be responsible for irregularities in the observed bands.

B. Negative-parity bands

1. Bands 9, 10, 4, and 5

The calculated low-spin bands of negative parity must be assigned to configurations with four dg protons and an odd number of $h_{11/2}$ neutrons. The lowest bands of this type have five $h_{11/2}$ neutrons; i.e., the [40,65] configuration. This is the configuration assigned to bands 9 and 10, where the lowest observed state has $I = 11/2$ because of decoupling. This is consistent with the configuration assigned to the bands 9 and
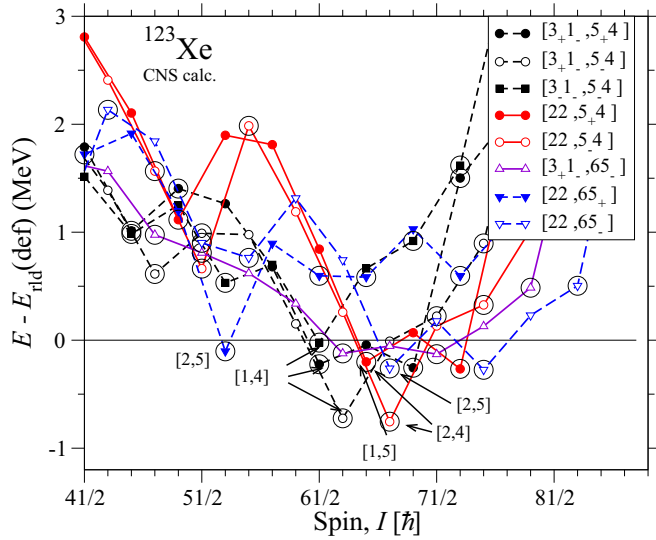
FIG. 10. Calculated excitation energies relative to a rotating liquid-drop energy for terminating configurations in ^{123}Xe. The states with spin vectors aligned along the oblate symmetry axis are highlighted by large open circles. Some low-energy terminating states are marked by the number of protons and neutrons in $h_{11/2}$ orbitals in their configurations.

10 in previous work [29,30]. The experimental energy levels are compared with the calculated ones in Fig. 11. The general features of the difference curves come out as expected when pairing is not included; i.e., they lie rather close to the average difference curve for all bands in ^{123}Xe. The average curve has been calculated with a least square fit of the differences to the function, $a \exp(-bI) - c$. The bands 6–8 and the highest spin values in band 16 have not been included in the fit. The resulting constants are $a = 3.05$ MeV, $b = -0.069\hbar^{-1}$ and $c = 1.12$ MeV. The decrease with spin I for the difference curve indicates the expected decrease of pairing energy with increasing spin.

The calculated deformation for the lowest-energy [40,65] band is close to $\gamma = -50°$ up to $I = 47/2$ where it jumps to $\gamma \approx 0°$. This shape change leads to a small alignment but is insufficient to explain the observed alignment gain at $I \approx 35/2$ in band 9. Furthermore, the shape change occurs at much higher spin than the observed crossing frequency of $\hbar\omega \simeq 0.5$ MeV. Thus, it appears that this backbend in band 9 is caused by pairing, in this case with a pair of neutrons in the $h_{11/2}$ shell, where the Fermi level is rather low in the shell, namely on the third level, corresponding to the [532]5/2 state at a prolate shape.

The spins of the bands in ^{123}Xe are plotted as a function of γ-ray energy in Fig. 12. The slope of the curves represents the dynamic moments of inertia, $\mathcal{J}^{(2)}$, of the bands. The alignment gain of $i \simeq 6\hbar$ for a pair of $h_{11/2}$ neutrons in band 9 appears larger than expected, considering that a similar alignment is observed in ^{123}Cs [7] for a band having an even number of $h_{11/2}$ neutrons. The comparison suggests that some shape change is also involved in the alignment of band 9 of ^{123}Xe. Band 10 appears to be the signature partner of band 9. An indication of a configuration change is also observed in this band at a frequency similar to that observed in band 9.
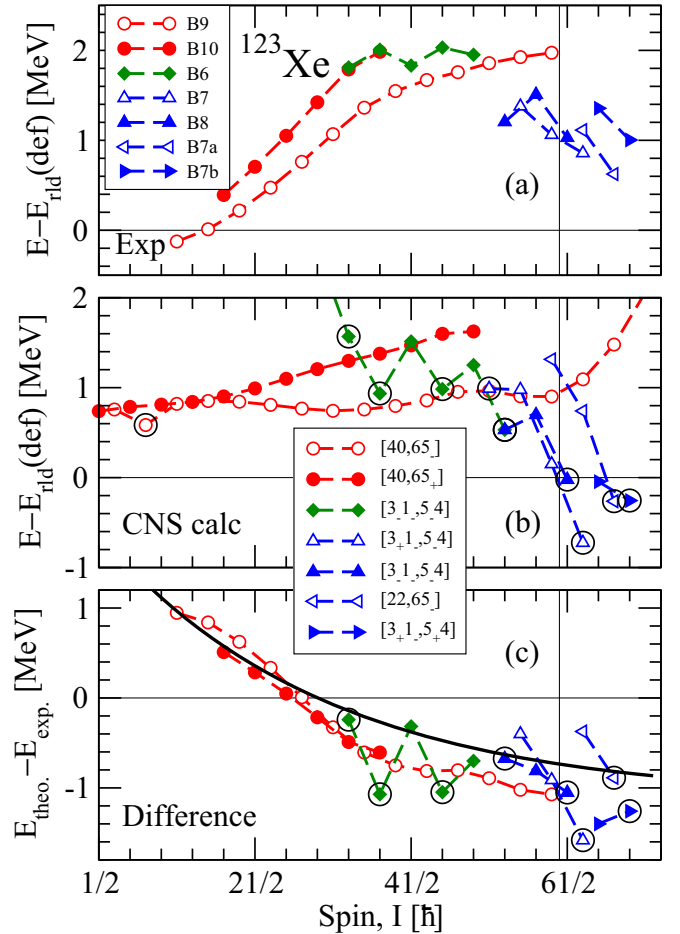

FIG. 11. Energies, relative to a rotating liquid-drop energy, for (a) the observed bands in ^{123}Xe, (b) calculated bands, (c) difference between experiment and calculations. The smooth curve in the lower panel is the average difference between experiment and calculations; see text for details.

Another pair of negative-parity bands, bands 4 and 5, has been observed at low energy: these are placed around 600 keV above the yrast band. Decay transitions have been observed from both bands to the yrast negative-parity band 9. Similar bands have been observed in neighboring, odd-N Xe isotopes. In particle-rotor calculations with a triaxial deformation of $\gamma = 20°$–25°, such bands are well understood as excited bands relative to bands 9 and 10 [30,39]. It seems that, with the rather large γ deformation, the $K = 2$ band of the triaxial core appears at low energy; see, e.g., Chap. 7 in Ref. [40], and it is mainly the coupling to this $K = 2$ band which results in bands 4 and 5. This assignment appears consistent with the suggestion that these bands in ^{121}Xe [25] and ^{125}Xe [27] are built on a $\nu h_{11/2}$ configuration coupled to the γ vibrational band of the even-even core [26]. With this assignment, these bands cannot be described in the present cranking approach.

2. Bands 1, 2, and 3

The bands 1–3 start at higher spin with an alignment of nearly $9\hbar$. This large initial alignment indicates a three-quasiparticle configuration for the bands. Thus, their most likely configuration has an odd number of protons in the dg
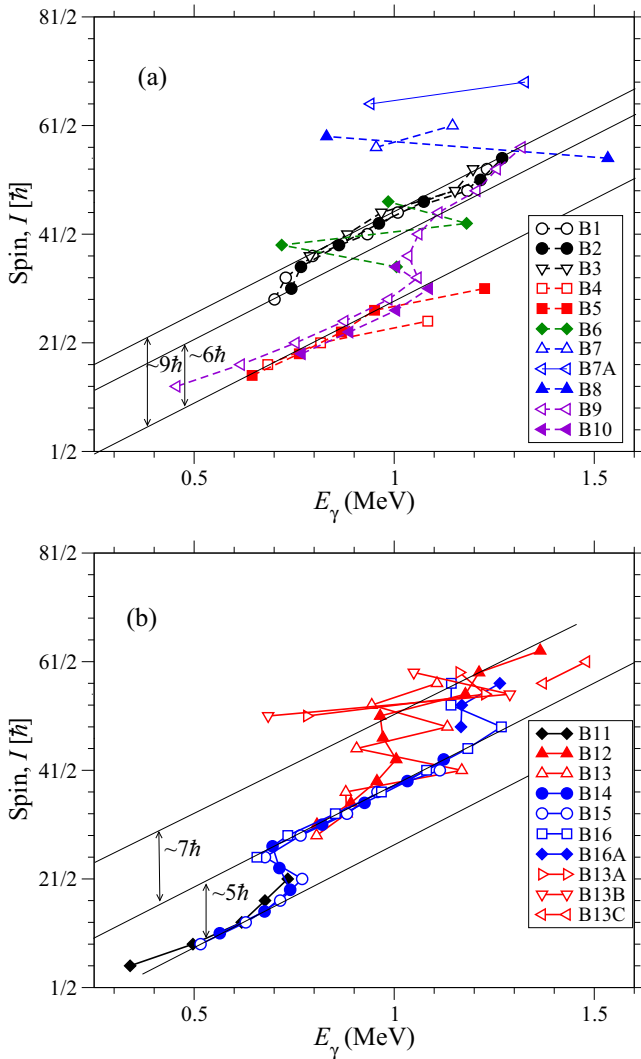
FIG. 12. Spins of states plotted as a function of γ-ray energy for the (a) negative- and (b) positive-parity bands observed in ^{123}Xe.

FIG. 13. Same as Fig. 11 but for bands 1, 2, and 3.

and $h_{11/2}$ orbitals, respectively; i.e., three dg and one $h_{11/2}$ protons. To end up with negative parity, there must be an even number of $h_{11/2}$ neutrons involved. In the CNS calculations, the configuration with six neutrons, [31,76], is found to be lowest in energy. The four bands which are formed from the two signatures of the dg protons and neutrons are drawn in Fig. 13. In these configurations, there is competition between minima at $\gamma \approx 0°$ and $\gamma \approx 40°$, where the latter lies slightly lower in energy. However, it seems likely that the more collective close-to-prolate minimum is observed in the experiment. Therefore, the energy at this minimum is compared with experiment in Fig. 13, where it is gratifying that all differences are close to the average value. For the configuration [3$_{-}$1, 7$_{-}$6], it is observed in the figure that the energies for $I =$ 33/2–49/2 are somewhat lower than the smooth trends seen for the other bands. This is because, for this configuration, there is no local minimum at $\gamma \approx 0°$ for these spin values and these energies correspond to the less-collective minimum at $\gamma \approx 40°$. Indeed, the absence of a prolate minimum over an
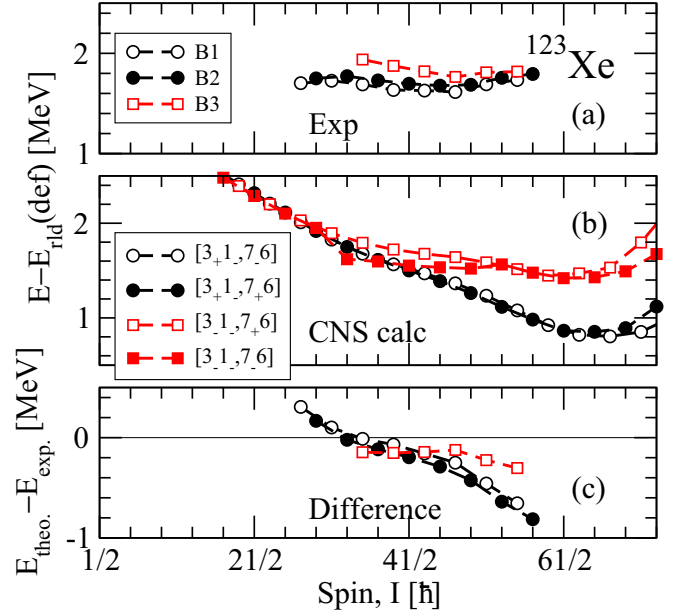
extended spin range for this configuration might explain why it has no experimental counterpart in the present level scheme.

3. Bands 6, 7, 7A, 7B, and 8

The bands 7, 7A, 7B, and 8 are low in excitation energy and decrease with increasing spin just above $I = 55/2$ [see Fig. 11(a)]. This suggests that they terminate in favored configurations. This is supported by the fact that they correspond to the spin values associated with the maximum spin in the valence configuration space. The favored negative-parity valence space configurations are [31,54] and [22,65] with $I_{max} = 63/2$ and 67/2, respectively. These are the highest spin values observed in bands 7 and 7A, respectively. They correspond to the lowest energies at high spin for all observed bands in Fig. 8. It thus seems natural to assign bands 7 and 7A to the [31,54] and [22,65] configurations. Experiment and calculations are compared in Fig. 11. For band 7, the difference between experiment and calculations is, on average, somewhat lower than expected and lies below the average values. The [22,65] configuration, on the other hand, is calculated somewhat higher than expected. Such discrepancies could, however, be cured by changing the rather uncertain position of the j shells. The fact that the calculated slope of the E-E_{rld} curves is considerably steeper in calculations than in experiment is of more concern. This means, for example, that the fully aligned $63/2^-$ state, which stands out as particularly favored in Fig. 10, is calculated too low compared with the highest-spin state observed in band 7.

The energies at high spin and the presence of linking $M1$ transitions suggest that band 8 is a signature partner of band 7, where the energy of the $61/2$ state lies at a similar energy if either the signature of the dg proton or that of the sd neutron is changed. It turns out that the full band 8 is better described by the signature change for the dg proton. Therefore, the [3$_{-}$1$_{-}$, 5$_{-}$4] configuration is compared with band 8

in Fig. 11. With this assignment, also the low energy of the $I =$ 53/2 state is described by an aligned configuration with one anti-aligned spin vector. Thus, compared with the fully aligned $I = 63/2$ state, one proton is moved from the $dg\,m_i =$ 5/2 to the $m_i = -5/2$ orbital; see Fig. 9. This 53/2$^-$ state is relatively low in energy in Fig. 10, but note that the 53/2$^-$ state of the [2,5] configuration, which has an anti-aligned $h_{11/2}$ neutron, is calculated to be even lower in energy.

Band 7B is also down-sloping and low in energy at high spin; see Fig. 8. As seen in Fig. 11, its energy is well described by a [31,54] configuration. In this configuration, a neutron is excited from the $dg\,m_i = -5/2$ orbital to the $sd\,m_i = 1/2$ state relative to the closed-core $I = 63/2$ state. The highest-spin state of band 7B, $I = 69/2$, corresponds to the I_{max} state of the $\alpha = 1/2$ [31,54] configuration with one hole in the $N = 64$ core. All in all, with the present assignments, bands 7, 7A, 7B, and 8 are rather well described, on average. On the other hand, the rather large fluctuations of the differences between calculations and experiment for these bands suggest that these low-collectivity configurations are somewhat difficult to calculate in the present pure cranking formalism.

Bands 7 and 8 are feeding into band 6, and this suggests that this band is associated with a similar configuration. On the other hand, it is very irregular and, as seen in Fig. 8, observed at a relatively high excitation energy. Thus, it is difficult to propose a reliable assignment. In any case, it is compared with the same [31,54] configuration as assigned to band 8 in Fig. 11. It turns out that the energy difference between experiment and calculation appears close to the average value, but the staggering is out of phase. Therefore, as expected, only a very qualitative assignment to band 6 can be proposed.

C. Positive-parity bands

Lower-spin, positive-parity states are built with the odd neutron in the sd ($s_{1/2}d_{3/2}$) and dg ($d_{5/2}g_{7/2}$) $\mathcal{N} = 4$ shells, keeping valence protons in the dg orbitals. As seen in Fig. 1, for a prolate shape, the odd proton occupies the [411]1/2, [402]5/2, or [404]7/2 Nilsson orbital. Higher-spin states can be generated by exciting a proton to the $h_{11/2}$ state with an odd number of neutrons in the $h_{11/2}$ orbital. Finally, close to the maximum-spin state in the valence space, configurations with two $h_{11/2}$ protons and, thus, with positive parity for the neutrons, might become competitive in energy. In the following, the positive-parity bands are first compared with similar bands in neighboring nuclei and possible configurations are discussed. The configurations are then assigned by comparing experimental results with those based on the CNS calculations.

1. Bands 11, 14, and 15

The positive-parity spin 3/2 state, which is assigned to band 11 in Fig. 2, and the 1/2$^+$ ground state [see Fig. 3] were known from previous work [28,29]. They can be described as the bandheads of a [411]1/2 band, see Fig. 1, even though they are best described with a rather large triaxiality, $\gamma = 20°$–25° [30]. Similar bands have been observed in the neighboring ^{121}Xe [25] and ^{125}Xe [27] isotopes.
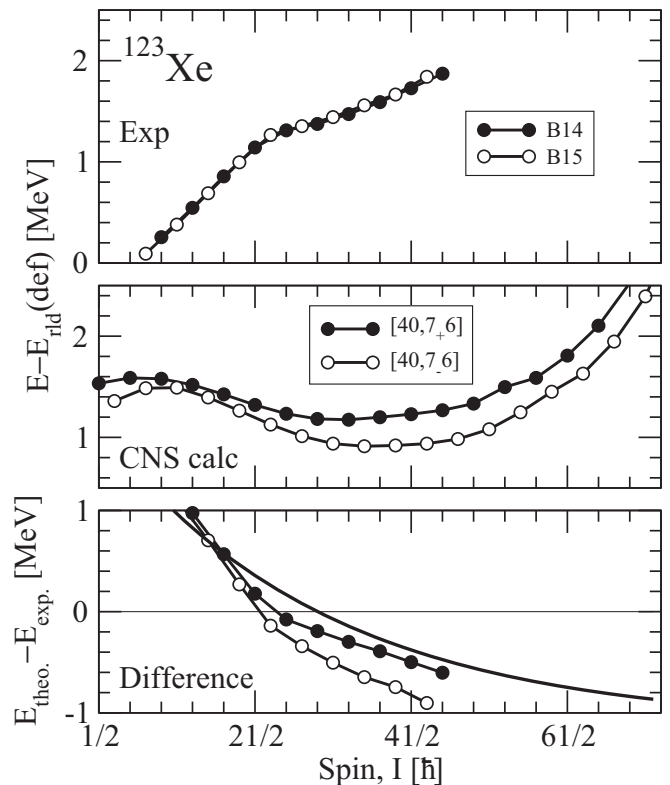

FIG. 14. Same as Fig. 11 but for bands 14 and 15, labeled as [404]7/2 in Fig. 8.

Another set of positive-parity bands starts at lower energy, bands 14 and 15; these are the positive-parity yrast bands for spin values $I = 7/2$–21/2, see Fig. 8. These bands and similar ones in neighboring nuclei, ^{121}Xe and ^{125}Xe, can be approximately described as built on the [404]7/2 orbital [30,39]. They exhibit a band crossing at $\hbar\omega \simeq 0.35$ MeV with an alignment gain of 5$\hbar$ (see Fig. 12). The crossing frequency and the amount of alignment gain indicate that alignment of a pair of $h_{11/2}$ neutrons is taking place. Therefore, the configuration of the band beyond the band crossing can be described as containing two aligned $h_{11/2}$ neutrons. Finally, a band which is best described as based on the [402]5/2 orbitals has also been observed [30], see Fig. 8. The general structure of the low-spin positive-parity bands built on $I = 1/2$, 5/2, and 7/2 bandheads, see Fig. 8, makes it natural to refer to them as [404]7/2, [402]5/2, and [411]1/2 bands, respectively. However, these bands are strongly mixed and, similar to the negative-parity bands, they are best described as associated with a rather large triaxiality [30,39].

The lowest-energy CNS configurations calculated with the odd neutron in a positive-parity state and no broken pairs for the protons is [40,76]. The calculated energies for this configuration are compared with the observed bands 14 and 15 in Fig. 14. The lowest minimum of the [40,76] configuration is calculated at $\gamma \approx -40°$ in an extended spin range approaching $I = 61/2$. This γ value corresponds to a triaxial shape with oblate character, while the general character of the low-spin positive-parity bands discussed above rather suggests a prolate character. Even so, one achieves general

agreement between observed and calculated energies; see Fig. 14. According to the discussion above, the other positive-parity low-spin bands are built on the same CNS configuration, but with the odd particle in another positive-parity orbital. Thus, they correspond to excited bands within the [40,76] configuration. Such configurations are difficult to calculate and, in any case, they would correspond to a very rough approximation of the true energies. Therefore, these bands will not be calculated here.

2. Bands 12, 13, and 16

The positive-parity bands observed at somewhat higher spin values are 12, 13, and 16. They should be assigned to three quasiparticle configurations; i.e., with one $h_{11/2}$ proton and with the odd neutron occupying an $h_{11/2}$ orbital as well. The lowest configuration is then [31,65] (see Fig. 1), which is compared with bands 12 and 13 in Fig. 15. It is instructive to follow the shape evolution in this configuration, as illustrated in the potential-energy surfaces in Fig. 16. There are essentially three minima in these surfaces. The one which is more or less noncollective (with γ close to 60°) is labeled III and calculated to be low in energy for all spin values. However, the smooth character of the bands indicates that collective configurations are likely observed at low spin. Such collective configurations are formed at $\gamma \approx -45°$ and $\gamma \approx 0°$, with the negative-γ minimum, labeled I, being lowest at low spins. But the minimum close to prolate shape, labeled II, is taking over around $I = 41/2$. This prolate minimum stays at $\gamma = 0°–15°$ over a large spin range before it finally terminates in a configuration which is rather high in energy at $I = 77/2$,

$$\pi \left[(dg)^3_{15/2} (h_{11/2})^1_{11/2} \right]_{13} \nu \left[(dg)^{-2}_6 (h_{11/2})^5_{35/2} (sd)^2_2 \right]_{51/2}.$$

Note that the distribution of the $\mathcal{N} = 4 \, dg$ and sd orbitals is not specified in the configuration labels. Thus, there are aligned [31,65] states which are more favored in energy at lower spins, especially the one with a closed $N = 64$ core,

$$\pi \left[(dg)^3_{15/2,17/2} (h_{11/2})^1_{11/2} \right]_{13,14} \nu (h_{11/2})^5_{35/2},$$

as seen from the low energy of these $I = 61/2, 63/2$ states in Fig. 15 (and in Fig. 10 for the 63/2 state of the $[3_+1_-, 65_-]$ configuration). Other noncollective states at rather favored energies are formed with one neutron excited across the $N = 64$ gap ($I = 69/2$) or with one anti-aligned dg proton ($I = 51/2, 53/2$).

Comparing with the CNS calculations, the observed bands 12 and 13 are well described by the $[3_\pm 1_-, 65_-]$ configuration at minimum I up to spin values around $I = 41/2$, then by the same configuration within minimum II and, finally, for the highest-spin states in band 12, possibly by the noncollective configurations associated with minimum III. Thus, in the calculations, there are low-energy favored terminations at $I = 53/2, 61/2$, and 69/2, while in band 12, these states are slightly more favored in energy than the $I = 57/2, 65/2$ ones. Another possibility is that the aligned states are situated somewhat higher in energy than the more collective ones in minimum II, but that there is an interaction between the states in minima II and III, so that the levels in minimum II
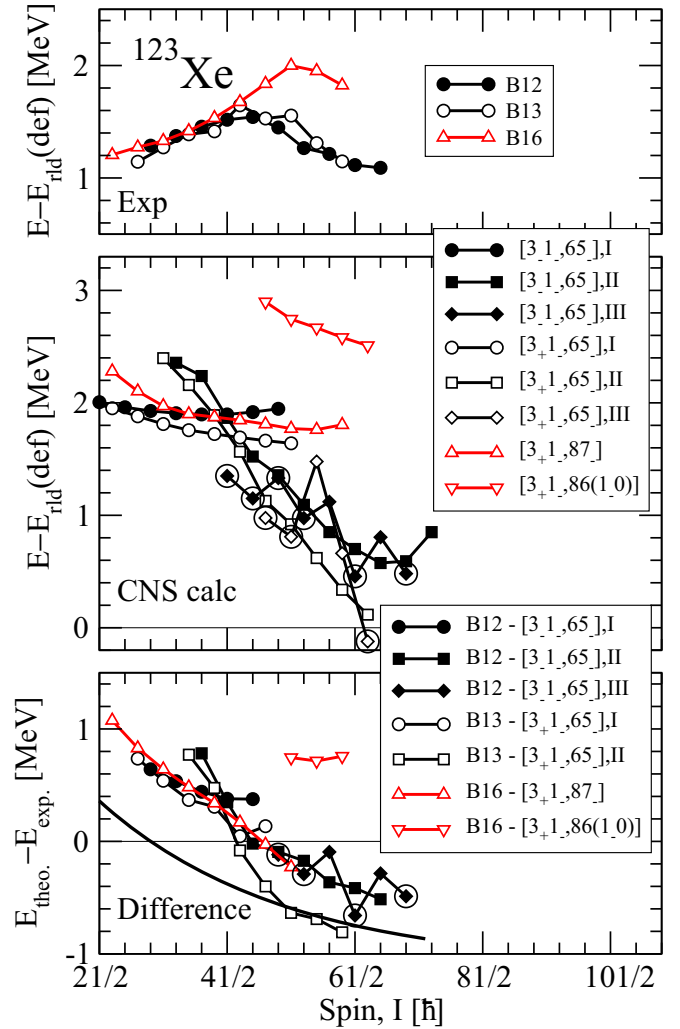

FIG. 15. Similar to Fig. 11 but for bands 12, 13, and 16. The energies for the [1,5] configuration have been calculated at three different minima in the total-energy surface (see Fig. 16) (I) $\gamma \simeq -45°$, (II) $\gamma \simeq 0°$, (III) $\gamma \simeq 60°$. The configuration suggested for the highest-spin state in band 16 has one hf and no $i_{13/2}$ neutron, as specified by the numbers in parentheses.

are pushed down by the favored noncollective states. Such interactions have been discussed for configurations which are analogous to the present neutron configurations; i.e., with a few protons in $h_{11/2}$ orbitals outside a $Z = 64$ core [41].

It is also interesting that the band crossing at $I \approx 41/2$ is described by the present unpaired calculations as caused by a jump in deformation from minimum I to minimum II; i.e., from a close-to-oblate collective minimum to a close-to-prolate collective one. It turns out that, in the crossing band in minimum II, the proton contribution to the spin is considerably larger than for the band with close-to-oblate deformation. This can be understood from the fact that the protons are located in the beginning of a shell and are much easier to align for $\gamma > -30°$ than for $\gamma < -30°$. This is true for the $h_{11/2}$ proton which becomes almost fully aligned at low frequencies; see, e.g., Fig. 28 of Ref. [42]. Thus, at the
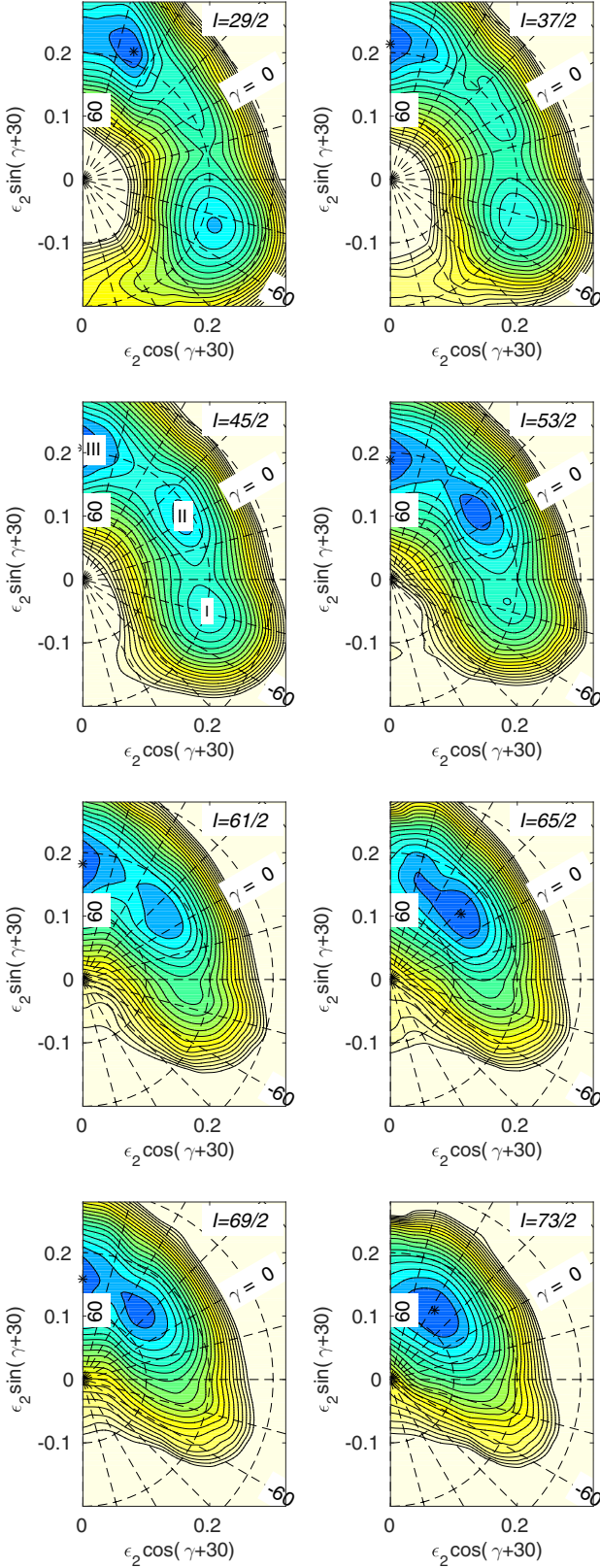
FIG. 16. Calculated total-energy surface for the [31,65] configuration of ^{123}Xe in the spin range $I = 29/2$–$73/2$. The three minima, I, II, and III at $\gamma \simeq -45°$, $\gamma \simeq 0°$, and $\gamma \simeq 60°$, which become lowest at different spin values, are labeled in the $I = 45/2$ energy surface. The contour line separation is 0.25 MeV.

frequency of the crossing, it contributes with only around $2\hbar$ in minimum I, but with more than $5\hbar$ in minimum II.

Band 16 starts at spin 23/2 and exhibits decays to band 15 as well as to band 11. An initial alignment of $6\hbar$ suggests a three quasiparticle configuration. One might guess that it is also built on a [31,65] configuration and associated with a signature $\alpha = 1/2$ for the $h_{11/2}$ neutrons. This configuration is, however, calculated somewhat too high in energy and band 16 is rather described by a [31,87] configuration; see Fig. 15. To understand the band crossing at $I \approx 51/2$, it seems appropriate to compare with the heavier region with protons instead of neutrons outside a closed Z, $N = 64$ core. In this region, such band crossings are caused by a jump of an $h_{11/2}$ proton to an fh orbital coming from the subshells located above the gap for particle number 82; see, e.g., Ref. [43]. An analogous configuration with one neutron in fh orbitals is drawn in Fig. 15. Comparing with the upper states in band 16, it has the correct slope in the $E\text{-}E_{rld}$ plot (correct alignment), but is calculated almost 1 MeV higher in energy. This would be remedied if the fh subshells were placed lower in excitation. Since their exact position is rather uncertain, this appears to be a rather plausible interpretation for the highest-spin states in band 16. Note also that there is a similar branch labeled band 16A in the level scheme. This sequence might be described as another signature combination associated with the same [31,86(10)] configuration.

D. Possible octupole correlations

It has been observed in nuclei of the mass-125 region [25,44–47] that one of the positive-parity bands decays to the yrast negative-parity band through several $E1$ transitions. The transition strength, $B(E1)$, of the order of 10^{-4} W.u., has been measured for these transitions. This is comparable to those observed in neutron-rich Ba ($Z = 56$, $N \simeq 88$) nuclei, where enhanced octupole collectivity has been reported [48,49]. Furthermore, it has been shown by Cottle *et al.* [50] that the shell structure in the $Z \simeq 56$ and $N \simeq 66$ region exhibits features similar to those seen in the lanthanide and actinide regions, where octupole correlations have been observed. In the mass-125 region, enhanced $B(E1)$ transition rates have been measured in ^{125}Ba [45], ^{121}Xe [25], ^{122}Cs [46], and ^{124}Cs [47], confirming the above observations.

Octupole correlations in atomic nuclei are due to the interaction between nucleons in opposite-parity orbitals lying near the Fermi level whose angular momenta differ by $3\hbar$; see Fig. 2 of Ref. [51]. In this mass region, the interaction between neutrons in $h_{11/2}$ and $d_{5/2}$ orbitals leads to such correlations. In ^{123}Xe, several interband transitions of dipole character ($E1$) have been observed from the positive-parity bands 14–16 to the negative-parity bands 9 and 10. In the discussion above, the configuration of the negative-parity bands 9 and 10 was shown to involve an odd-number of neutrons in $h_{11/2}$ orbitals; i.e., [40,65], whereas lower spin-states of bands 14–16 can be described by the configuration [40,76]. The proton occupies gd shells in both configurations. Therefore, the presence of $\Delta l = 3$ neutron orbitals, $h_{11/2}$ and $d_{5/2}$, may lead to octupole correlations in this nucleus.

TABLE II. $B(E1)/B(E2)$ ratios and transition rates $B(E1)$ for some of the transitions of bands 14 and 15.

I^π	$E_\gamma(E1)$ (keV)	$E_\gamma(E2)$ (keV)	$I_\gamma(E1)/I_\gamma(E2)$	$B(E1)/B(E2)$ $(10^{-7}$ fm$^{-2})$	$B(E1)$ $10^{-4}\,e$ fm^2
Band 14					
$13/2^+$	818.6	563.5	0.42(4)	0.34(3)	1.47(13)
$17/2^+$	1038.3	675.8	0.40(6)	0.39(6)	1.8(3)
$21/2^+$	1160.9	739.6	0.54(6)	0.59(7)	2.9(3)
$25/2^+$	1120.8	712.4	0.43(6)	0.43(7)	2.2(4)
$29/2^+$	939.9	695.6	0.33(5)	0.49(7)	2.6(4)

The $B(E1)/B(E2)$ ratio [25]

$$\frac{B(E1; I \to I-1)}{B(E2; I \to I-2)} = \frac{1}{1.3 \times 10^6} \frac{E_\gamma^5(E2)}{E_\gamma^3(E1)} \frac{I_\gamma(E1)}{I_\gamma(E2)} \text{ fm}^{-2},$$

calculated from the intensities of the interband $E1$ transitions and intraband $E2$ transitions are listed in Table II.

Furthermore, the potential-energy surface calculated for the [40,76] configuration, which has been assigned to bands 14 and 15, shows a minimum at $\varepsilon_2 = 0.22$ and $\gamma \simeq -40°$. Considering the nuclear shape as triaxial with the above deformation parameters, the reduced transition probabilities, $B(E2)$, for the in-band transitions have been calculated following the formalism described in Refs. [52,53]. Finally, the reduced transition rates $B(E1)$ for the interband dipole transition have been calculated using the $B(E2)$ and the $B(E1)/B(E2)$ ratios, and are listed in the last column of Table II. The $B(E1)$ transition rates are of the same order as those observed for the bands in ^{125}Ba [45], ^{121}Xe [25], and ^{117}Xe [44], where octupole correlations have been suggested. The transition rates also increase with increasing spin. A discontinuity in the trend is observed around spin 25/2, which is likely due to a change of configuration at the band crossing.

V. SUMMARY

The high-spin structure of ^{123}Xe was studied in a heavy-ion-induced fusion-evaporation reaction with the Gamma-sphere spectrometer. The existing level scheme of ^{123}Xe was confirmed and significantly extended with the addition of five new bands and the placement of many interband transitions. The configurations of the bands have been discussed within the framework of CNS formalism. They involve excitations of neutrons within the $N = 50–82$ shells, except for the higher-spin states of band 16, where the excitation of one neutron across the $N = 82$ shell gap is proposed. A shape transition from triaxial at lower spin to prolate at higher spin has been suggested. The alignment gain observed in bands 12 and 13 can be explained by a shape transition from triaxial ($\gamma \simeq -45°$) at lower spin, to prolate ($\gamma \simeq 0°$) at medium spin, and possibly to oblate ($\gamma \simeq 60°$) at higher spin. These higher-spin states are due to noncollective excitations and the possibility of band termination has been discussed. Furthermore, it is suggested that bands 7 and 7A are extended to the maximum spin in the valence space for the $\pi(h_{11/2})^1\nu(h_{11/2})^4$ and $\pi(h_{11/2})^2\nu(h_{11/2})^5$ configurations, respectively, while band 7B is followed to the $I_{\max}$ state for a 1p-1h excitation relative to the $N = 64$ gap.

[1] A. Granderath *et al.*, Nucl. Phys. A **597**, 427 (1996).

[2] R. Wyss *et al.*, Nucl. Phys. A **505**, 337 (1989).

[3] S. G. Nilsson and I. Ragnarsson, *Shapes and Shells in Nuclear Structure* (Cambridge University Press, Cambridge, 1995).

[4] A. V. Afanasjev, D. B. Fossan, G. J. Lane, and I. Ragnarsson, Phys. Rep. **322**, 1 (1999).

[5] W. Lieberz *et al.*, Phys. Lett. B **240**, 38 (1990).

[6] V. Werner *et al.*, Nucl. Phys. A **692**, 451 (2001).

[7] A. K. Singh *et al.*, Phys. Rev. C **70**, 034315 (2004).

[8] H. Timmers *et al.*, J. Phys. G **20**, 287 (1994).

[9] A. Al-Khatib *et al.*, Phys. Rev. C **74**, 014305 (2006).

[10] A. Al-Khatib *et al.*, Eur. Phys. J. A **36**, 21 (2008).

[11] F. Seiffert *et al.*, Nucl. Phys. A **554**, 287 (1993).

[12] C. Rønn Hansen, G. Sletten, G. B. Hagemann, B. Herskind, D. R. Jensen, P. Bringel, C. Engelhardt, H. Hubel, A. Neusser-Neffgen, A. K. Singh, M. P. Carpenter, R. V. F. Janssens, T. L. Khoo, T. Lauritsen, P. Bednarczyk, T. Byrski, D. Curien, G. Benzoni, A. Bracco, F. Camera, S. Leoni, R. M. Clark, P. Fallon, A. Korichi, J. Roccaz, A. Maj, J. N. Wilson, J. C. Lisle, T. Steinhardt, O. Thelen, and S. W. Odegaard, Phys. Rev. C **76**, 034311 (2007).

[13] I. Ragnarsson *et al.*, Phys. Scr. **34**, 651 (1986).

[14] A. O. Evans *et al.*, Phys. Rev. Lett. **92**, 252502 (2004).

[15] E. S. Paul *et al.*, Phys. Rev. Lett. **98**, 012501 (2007).

[16] S. Nag *et al.*, Phys. Rev. C **90**, 037302 (2014).

[17] S. Nag *et al.*, Phys. Rev. C **88**, 044335 (2013).

[18] P. Singh *et al.*, Phys. Rev. C **85**, 034319 (2012).

[19] P. Singh *et al.*, Phys. Rev. C **82**, 034301 (2010).

[20] P. Singh *et al.*, Phys. Rev. C **85**, 054311 (2012).

[21] E. S. Paul *et al.*, J. Phys. G **19**, 913 (1993).

[22] S. Nag *et al.*, Phys. Rev. C **94**, 034307 (2016).

[23] P. Singh, *et al.*, Phys. Rev. C **84**, 024316 (2011).

[24] P. Singh, *et al.*, Phys. Rev. C **86**, 067305 (2012).

[25] J. Timár *et al.*, J. Phys. G **21**, 783 (1995).

[26] M. Serris *et al.*, Z. Phys. A: Hadrons Nucl. **358**, 37 (1997).

[27] A. Al-Khatib *et al.*, Phys. Rev. C **83**, 024306 (2011).

[28] A. Luukko *et al.*, Nucl. Phys. A **357**, 319 (1981).

[29] A. Schmidt *et al.*, Eur. Phys. J. A **2**, 21 (1998).

[30] A. Gade *et al.*, Nucl. Phys. A **686**, 3 (2001).

[31] I. Y. Lee, Nucl. Phys. A **520**, c641 (1990).

[32] D. C. Radford *et al.*, Nucl. Phys. A **545**, 665 (1992).

[33] S. Ohya, Nucl. Data Sheets **102**, 547 (2004); National Nuclear Data Centre, Brookhaven National Laboratory, USA, https://www.nndc.bnl.gov/ensdf

[34] G. Rainovski *et al.*, Phys. Rev. C **66**, 014308 (2002).

[35] T. Bengtsson and I. Ragnarsson, Nucl. Phys. A **436**, 14 (1985).

[36] B. G. Carlsson and I. Ragnarsson, Phys. Rev. C **74**, 011302 (2006).

[37] K. Pomorski and J. Dudek, Phys. Rev. C **67**, 044316 (2003).

[38] Hai-Liang Ma, B. G. Carlsson, I. Ragnarsson, and H. Ryde, Phys. Rev. C **90**, 014316 (2014).

[39] A. Gelberg, D. Lieberz, P. von Brentano, I. Ragnarsson, P. B. Semmes, and I. Wiedenhöver, Nucl. Phys. A **557**, 439c (1993).

[40] J. M. Eisenberg and W. Greiner, *Nuclear Theory* (North-Holland Publishing Company, Amsterdam, 1970, 1975), Vol 1.

[41] M. A. Riley, J. D. Garrett, J. F. Sharpey-Schafer, and J. Simpson, Phys. Lett. B **177**, 15 (1986).

[42] G. Andersson *et al.*, Nucl. Phys. A **268**, 205 (1976).

[43] A. Kardan, I. Ragnarsson, H. Miri-Hakimabad, and L. Rafat-Motevali, Phys. Rev. C **86**, 014309 (2012).

[44] Z. Liu *et al.*, Eur. Phys. J. A **1**, 125 (1998).

[45] P. Mason *et al.*, Phys. Rev. C **72**, 064315 (2005).

[46] S. Sihotra *et al.*, Phys. Rev. C **78**, 034313 (2008).

[47] K. Selvakumar *et al.*, Phys. Rev. C **92**, 064307 (2015).

[48] G. A. Leander, W. Nazarewicz, P. Olanders, I. Ragnarsson, and J. Dudek, Phys. Lett. B **152**, 284 (1985).

[49] W. R. Phillips, I. Ahmad, H. Emling, R. Holzmann, R. V. F. Janssens, T.-L. Khoo, and M. W. Drigert, Phys. Rev. Lett. **57**, 3257 (1986).

[50] P. D. Cottle, K. A. Stuckey, and K. W. Kemper, Phys. Lett. B **219**, 27 (1989).

[51] Nazarewicz *et al.*, Nucl. Phys. A **429**, 269 (1984).

[52] A. Görgen *et al.*, AIP Conf. Proc. **764**, 9 (2005).

[53] K. Selvakumar *et al.*, Phys. Rev. C **88**, 024313 (2013).